UNIVERSITY OF
CAMBRIDGE
Department of Computer
Science and Technology

CARICO: Scheduling via Federated Workload Capacity Estimation

Luca Choteborsky

Selwyn College

June 2025

Submitted in partial fulfillment of the requirements for the
Computer Science Tripos, Part III

Total page count: ??

Main chapters (excluding front-matter, references and appendix): 53 pages (pp 10–62)

Main chapters word count: 467

Methodology used to generate that word count:

[For example:

```
$ make wordcount
gs -q -dSAFER -sDEVICE=txtwrite -o - \
   -dFirstPage=6 -dLastPage=11 report-submission.pdf | \
egrep '[A-Za-z]{3}' | wc -w
467
```

]

Declaration

I, Luca Choteborsky of Selwyn College, being a candidate for Part III of the Computer Science Tripos, hereby declare that this report and the work described in it are my own work, unaided except as may be specified below, and that the report does not contain material that has already been used to any substantial extent for a comparable purpose. In preparation of this report, I adhered to the Department of Computer Science and Technology AI Policy. I am content for my report to be made available to the students and staff of the University.

Signed:

Date:

Abstract

Kubernetes is a widely-used open-source container orchestration system that automates the deployment, scaling and management of containerized applications. Efficient scheduling is a critical component of Kubernetes, dictating an optimal allocation of pods across nodes to maximise a set of goals. Kubernetes schedulers generally fall into two categories: pod-descriptive and telemetric-based. Pod-descriptive schedulers, like the default `kube-scheduler`, rely on accurately defined Pod resource requests for optimal performance. In contrast, telemetric-based schedulers leverage collected Node metrics to identify under or over-utilized Nodes. While these are often used to refine decisions made by existing pod-descriptive schedulers, this dissertation focuses on exploring the potential of a telemetric-only scheduler.

Scheduling in Kubernetes without explicit Pod resource requests remains largely unexplored due to its complexity. Traditional bin-packing approaches are insufficient; instead, a telemetric-only scheduler requires a novel strategy to derive optimal plans from collected telemetry.

Pronto offers a promising direction. This federated, asynchronous, and memory-limited algorithm schedules tasks across hundreds of workers. It enables individual workers to build local workload models from telemetry, which are then aggregated to form a global system view. For a telemetric-only scheduler, maximizing information aggregation is crucial. However, in very large clusters, centralizing all this data quickly becomes a bottleneck. By distributing the knowledge federation workload across the cluster, we can significantly reduce the load on a central scheduler.

Unfortunately, Pronto's direct application to Kubernetes proved unfeasible due to its communication latency assumptions and early empirical findings. Consequently, I propose Carico (Italian for "load"), a novel scheduler that shares Pronto's core properties but accounts for communication latency. Carico enables Nodes to perform Federated Singular Value Decomposition (FSVD) on capacity-based metrics, modeling past resource usage to estimate future workload capacity.

To evaluate Carico, I implemented a prototype within the Kubernetes ecosystem. This involved extensive investigation into various metrics and filters to generate a precise capacity signal. Finally, I benchmarked Carico's overall performance against the default

kube-scheduler on a Kubernetes cluster with diverse workloads. While Carico achieved comparable throughput, it significantly outperformed kube-scheduler as a QoS scheduler, demonstrating lower Pod Completion times and improved workload isolation.

Acknowledgements

This project would not have been possible without the wonderful support of ... [optional]

Contents

Chapter 1

Introduction

Datacenters serve as the foundational infrastructure for modern computing, housing hundreds of thousands of machines that underpin diverse user applications and data-parallel computations. The escalating demand for compute, memory, storage, and network resources necessitates increasingly large and complex datacenters. Within these environments, datacenter scheduling is a critical task: it involves allocating available resources to workloads to ensure performance objectives are met while maintaining high overall datacenter utilization. The difficulty of this problem is compounded by ever-increasing input workload rates, dynamically changing workload characteristics, and the heterogeneity of resources. Schedulers are expected to deliver short user response times, high resource utilization, and high scheduling throughput simultaneously, making it one of the most challenging aspects of datacenter operation.

To address these challenges, various scheduler architectures have emerged: i) centralised schedulers, such as Borg [] or Kubernetes [], that execute all scheduling logic from a sinle point, ii) decentralised schedulers [**?**] which aimed to solve central schedulers scalability issue by dividing the task of allocation across independent processes, and iii) distributed schedulers, like Sparrow [], which remove the need for coordination or shared state. Numerous algorithms have been devised to solve task scheduling. Multi-dimensional resource allocation simplifies scheduling to bin packing. While many schedulers [**? ?**] use user-provided job resource requests, the issue of inaccurate resource estimation has necessitated for more complex techniques []. On the other hand, other schedulers aim to predict the availability of node resources. These schedulers initially consisted of those that probed a portion of the datacenter on-demand, and those that performed offline machine learning on telemetry from the entire datacenter. As a result, these methods had to trade responsiveness for a holistic model of the datacenter.

Kubernetes has firmly established itself as the leading platform for container orchestration, experiencing widespread adoption across diverse industries and organizations of all scales [1]. From stateless microservices to complex stateful databases, Kubernetes serves

as the infrastructure backbone for cloud computing services like Google Cloud [2] and Azure [3]. Its versatility, from supporting machine learning (ML) deployments [4], edge computing [5] end serverless functions [6, 7], solidifies Kubernetes' position as a cornerstone of the cloud-native industry.

A core function of container orchestration is the efficient scheduling of containers across a cluster. In this dynamic and resource-intensive landscape, efficient online scheduling is paramount for both performance and cost-effectiveness. Poor scheduling decisions can lead to significant infrastructure waste, directly impacting an organization's bottom line. Misconfiguration in resource requests and limits is a primary cause of under-utilised resources or idle nodes, leading to higher billing [8, 9].

Kubernetes was built upon the ideas from Borg [], a large-scale cluster management developed and used by Google. Consequently, Kubernetes' default scheduler [10] (`kube-scheduler`) performs bin-packing based on the resource requests included in Pod descriptions and heuristic-based capacities calculated from the Nodes' advertised hardware. The performance achieved by `kube-scheduler` therefore depends on accurate estimates of Pod resource usage. While telemetry-based systems have been proposed to improve scheduling decisions, they often use expensive deep-ML techniques [11, 12] or focuses on a per-Node level [13]. These telemetry-based systems typically augment existing resource requests or re-schedule already running workloads to less congested Nodes.

Pronto [14] offers a promising direction for a purely telemetry-driven approach. This novel federated, asynchronous, and memory-limited algorithm allows each compute node to work with a global view of the system by distributing the knowledge federation workload to reduce the burden on a central scheduler. However, its direct application within a Kubernetes scheduling environment faces significant challenges. Pronto's original design assumes zero communication latency and yields only a binary "Reject-Job" signal, which lacks the granularity for sophisticated Node scoring and fails to account for significant Pod startup latencies observed in real-world Kubernetes clusters [15]. Furthermore, empirical investigations into Linux Pressure Stall Information (PSI) metrics, a potential replacement for the VMware vSphere CPU-Ready metric, revealed frequent transient spikes attributed to the container runtime. This would make it difficult to efficiently distinguish genuine resource contention from noise when collecting a small set of metrics. These limitations necessitate a more sophisticated signal that is both **comparable** for effective Node ranking and **reservable** to track the pending impact of in-flight Pods.

1.1 Dissertation Aims and Contributions

This dissertation aims to apply the theory behind Pronto within the Kubernetes ecosystem by proposing, implementing, and evaluating CARICO (Italian for "load"), a novel, purely telemetry-driven scheduling algorithm that maintains the federated, asynchronous,

and memory-limited properties of PRONTO explicitly accounting for communication latency.

The key contributions of this project are:

- **Feasibility Analysis of Pronto for Kubernetes:** An investigation into the applicability of PRONTO's principles to Kubernetes scheduling, highlighting its flawed assumptions and presenting empirical evidence for the challenges of using raw telemetry metrics.
- **Proposal of CARICO:** A novel federated, asynchronous, and memory-limited scoring algorithm that explicitly accounts for communication latency.
  - Novel application of Federated Singular Value Decomposition (FSVD) to build a local model of recent resource usage, adapting the standard SVD subspace merge operation for a lack of mean-centering.
  - Presentation of a novel **comparable** capacity signal that scores a Node's predicted ability to accept new workloads, considering recent resource utilisation across the cluster.
  - Application of simple signal processing techniques to transform the generated capacity signal into a **reservable** metric, enabling schedulers to account for communication latencies.
- **Prototype Implementation and Evaluation of CARICO:**
  - Extensive investigation into different telemetry metrics and signal processing techniques within the setting of a Kubernetes cluster to generate an accurate and precise capacity signal.
  - Analysis of the correctness of the generated signal and exploration of approaches for estimating reservation quantities.
  - Comprehensive evaluation of CARICO's overall performance under various workloads on a real-world Kubernetes cluster, comparing its throughput, Quality of Service (QoS), and performance isolation against the industry-standard `kube-scheduler`.

1.2 Dissertation Overview

The remainder of this dissertation is structured as follows:

- **Chapter 2 (Background):** This chapter provides foundational knowledge, detailing Kubernetes architecture and its scheduling mechanism. It introduces PRONTO, explaining its core mathematics and highlighting its accuracy in predicting performance degradation, while also critically examining its weaknesses that necessitate

a more sophisticated signal. Finally, it reviews existing Kubernetes schedulers to contextualize this work within the current landscape.

- **Chapter 3 (Design):** This chapter proposes the novel CARICO algorithm, providing detailed proofs and reasoning to explain the generation and properties of its capacity signal.
- **Chapter 4 (Implementation):** This chapter outlines the structure of the CARICO system within Kubernetes, exploring the selection of numerous metrics and signal processing techniques employed to generate an accurate and precise signal.
- **Chapter 5 (Evaluation):** This chapter presents a comprehensive evaluation of CARICO's performance under different workloads, collecting numerous performance metrics and comparing it against the standard `kube-scheduler`.
- **Chapter 6 (Conclusion and Future Work):** This final chapter summarizes the key findings of the dissertation and proposes potential directions for future research.

Chapter 2

Background

This chapter lays the groundwork for understanding the problem space addressed by this dissertation. I first explain how scheduling works in Kubernetes, providing the necessary context for the system architecture. Subsequently, the chapter delves into PRONTO, outlining its core concepts and the compelling motivations for exploring its application within the Kubernetes ecosystem. Finally, a review of related Kubernetes schedulers is provided to highlight the existing landscape and position this work within the current state of the art.

2.1 Datacenter Scheduling

Modern datacenters are physical facilities that serve as the backbone for running diverse user applications and data-parallel computations. The increasing demand for computing resources like compute, memory, storage and network necessitates for ever larger datacenters. Hyperscale datacenters provided by cloud providers like Google, Amazon, Microsoft, and Meta house hundreds of thousands fo machines [**?** **?**]. Datacenter scheduling is the fundamental task of allocating the available resource to workloads such that the their performance objectives are satisfied and the overall datacenter utilisation is kept high. Small deviations from the desired objectives can have substantial detrimental effects with millions of dallars in revenue potentially lost [**?**]. This problem continues to grow in difficulty. Modern schedulers must map the ever-increasing input workload rate and ever-changing workload characteristics onto heterogeneous resources [**?** **?**]. Moreover, they are expected to schedule for short user response time and high resource utilisation while also delivering high scheduling throughput [**?** **?** **?** **?** **?**]. This makes scheduling one of the most important and one of the most challenging aspects of datacenter operation.

Multiple scheduler designs have been proposed to tackle this vast problem space. Scheduler architectures can be classified into the following:

- **Centralised Schedulers:** Centralised schedulers like Borg [], Firmament [], Ku-

bernetes [], and Quincy [] consist of a single monolithic scheduler that executes the entire scheduling logic to place tasks on available resources []. This design allows for more sophisticated policies to be applied. Machines in the datacenter update their health and resources periodically, and this information is then used for subsequent allocations. To overcome the issue of a single point of failure (SOPF), centralised schedueleres are often configured in a highly available topology [**?** **?** **?**], where in the case of a failure, a leader election round is triggered.

Two-tiered scedulers are a variant of central schedulers where one entity (master) manages resources of the datacenter and their allocation, and the other carries out task placement. With Mesos [**?**], individual nodes offer available resources to the master which then offers these to individual application schedulers. This delegates resource allocation to schedulers with domain-specific knowledge, while still being able to handle node failures through the master.

- **Decentralised Schedulers:** As datacenters continue to grow, centralised schedulers become bottlenecks, facing increased overheads collecting resource information, while simultaneously handling high frequency job arrivals. To overcome this limitation, decentralised schedulers like Apollo [] and Omega [] employ several independent job schedulers which update a shared centralised state after each placement decision. Due to its concurrent nature, commits can result in conflicts [**?**] which must be handled carefully.

- **Distributed Schedulers:** Like decentralised schedulers, distributed schedulers have multiple indpendent scheduler instances. However, they require no coordination or shared state. Schedulers like Peacock [**?**] and Sparrow [**?**] aim to make scheduling decisions as fast as possible, without the knowledge of the entire datacenter. Although these schedulers are scalable and available owning to their distributed nature, having a limited view of the datacenter can result in sub-optimal placement choices.

- **Hybrid Schedulers:** Hybrid schedulers like Dice [**?**], Eagle [**?**], Hydra [**?**] and Mercury [**?**] combine the properties of centralised and distributed schedulers to achieve good placement at scale and for high workload arrival rates. They typically employ separate schedulers, each tasked with placing a different kind of job into specially reserved sub-clusters [**?** **?** **?** **?**]. Each scheduler uses different scheduling policies, typically prioritising short job placement for improved job completion times. Due to the requirement for workload-specific parameters, sub-clusters may become under- or over-utilised when workload characteristics change [**?**].

Much resarch has also gone into developing different algorithms for scheduling. **Multi-dimensional resource allocation** transforms scheduling into a bin-packing problem. Schedulers like Quincy [**?**] and Jockey [**?**] allocate a uniform amount of resources to

all tasks regardless of their needs, potentially hurting application performance. Other schedulers [? ? ? ?], support user-specified job resource requirements, but risk users overestimating [?] or not knowing howing much to request [?]. Several methods have been proposed to improve the accuracy of job resource requests: [?] profiles the job before actual execution, [? ?] decreases or redistributes the initial resource allocation after an observation period, [? ? ?] analyse historical traces of jobs to build a performance model of the expected performance based on the job resource allocation.

Constraint handling schedulers allows tasks to have placement constraints, such as, requiring specialist hardware like a Tensor Processing Units [?](TPUs). Kubernetes [] supports both hard (mandatory) and soft (not mandatory but preffered) constraints, as well as affinity/anti-affinity constraints.

Finally, schedulers like [? ? ? ? ? ? ?] rely on **predictions of node's future resource availablilty** to avoid saturation and efficently utilise resources across data center nodes. Approaches range from probing available nodes on an on-demand basis [? ? ?] to collectively generated telemetry across the datacenter and using offline machine learning prediction to tackle oversubscription [? ?]. While it has been shown that schedulers generate improved holistic models for efficient provision when given access to performance data from all data center nodes [? ? ? ? ? ?], they typically operate on a near offline fashion with a high network cost, making them slow to react in real-time to performance problems. PRONTO [14] pioneers a federated approach to analysing real-time telemetry from virtualised data center nodes for online task scheduling.

2.2 Kubernetes

2.2.1 Kubernetes Overview

A Kubernetes cluster consists of a control plane and one or more worker Nodes. Components in the control plane manage the overall state of the cluster. The `kube-apiserver` exposes the Kubernetes HTTP API, which is used to publish objects such as Deployments, DaemonSets and Jobs. Each Node in the cluster contains a `kubelet` which manages Pods and ensures they and their containers are running via a container runtime.

Kubernetes objects are persistent entities in the Kubernetes system. They act as "records of intent" and describe the cluster's desired state: once created, the Kubernetes system will constantly work to ensure that the objects exists. The Kubernetes API is used to create, modify or delete these Kubernetes objects. Almost every Kubernetes object includes two fields: `spec` and `status`. `spec` is used on creation as a description of the Objects desired state. Users can define affinities and QoS classes within this field to influence scheduling decisions. Containers also contain a `spec` field which specifies `request` and `limits`. The `request` field behaves as a set of minimum requirements and is used when

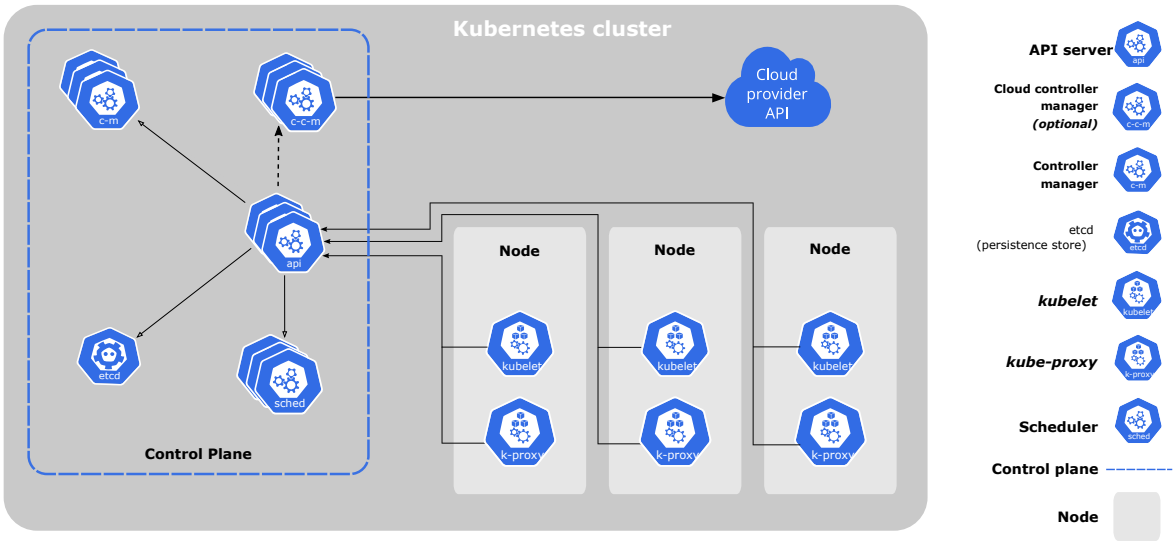

Figure 2.1: The components of a Kubernetes cluster [16]

scheduling Pods. In contrast, the `limits` field is used by kernel of the Node to throttle a container's resource usage. In Kuberentes, the resource units for `resource` and `limits` are the following:

- **CPU:** The metric used is *cpu* units, where 1 cpu unit is equivalent to a 1 physical/virtual core. Fractional requests are permitted with the notation xm; 100m can be read as "one hundred millicpu".
- **Memory:** This is measured in bytes. Kubernetes also allows the use of quantity suffixes, such as, k, M, G, Ki, Mi, Gi.

`status` describes the current state of the object, supplied and updated by the Kubernetes system. These fields are core to scheduling in Kubernetes.

2.2.2 Scheduling in Kubernetes

In Kubernetes, Pods are the smallest deployable units of computing that you can create and manage. It represents a single instance of a running process in your cluster and typically contains one or more containers that are tightly coupled and share resources. Pods can be individually created with their own Yaml files. However, the Kubernetes API also provides workload objects to manage multiple pods: these objects represent a higher abstraction level than a Pod, and the Kubernetes control plane uses the workload's specification to manage Pod objects on your behalf. Example workloads include Deployment, StatefulSet, DaemonSet and Job.

When a Pod is created, it initially exists in a "Pending" state: it has been declared but hasn't yet been allocated to a Node. Kubernetes schedulers watch for newly created but unassigned Pods, and based on a set of rules or algorithms, select the most suitable

Node for that Pod. Once a Node is chosen, the scheduler "binds" the Pod to the Node, updating the Pod's definition in the Kubernetes API server by setting its `spec.nodeName` field to the name of the Node. Once this occurs, the Pod transitions from "Pending" to "Running".

2.3 Pronto

2.3.1 Principle Component Analysis

This section first explains Singular Value Decomposition (SVD) and how it relates to solutions of Principal Component Analysis (PCA). I then introduce Incremental-SVD and Subspace-Merge, which are used to perform FPCA on the stream of telemetry produced by each Node.

2.3.2 Singular Value Decomposition

The SVD of a real matrix $\mathbf{A}$ with m rows and n columns where $m \geq n$ is defines as $\mathbf{A} = \mathbf{U}\Sigma\mathbf{V}^T$. Here, $\mathbf{U}$ and $\mathbf{V}$ are orthogonal matrices of shape $m \times m$ and $n \times n$ containing the left and right singular vectors, respectively. Σ is a rectangular matrix of shape $m \times n$ with singular values σ_i along its diagonal [17].

$$\mathbf{A} = \begin{bmatrix} a_{11} & \dots & a_{1n} \\ \vdots & \ddots & \vdots \\ a_{m1} & \dots & a_{mn} \end{bmatrix} = \begin{bmatrix} | & & | \\ u_1 & \dots & u_m \\ | & & | \end{bmatrix} \begin{bmatrix} \sigma_1 & & & | & & | \\ & \ddots & & 0 & \dots & 0 \\ & & \sigma_m & | & & | \end{bmatrix} \begin{bmatrix} — & v_1^T & — \\ & \vdots & \\ — & v_m^T & — \\ — & v_{m+1}^T & — \\ & \vdots & \\ — & v_n^T & — \end{bmatrix} \tag{2.1}$$

SVD can also be written compactly by discarding the elements which do not contribute to $\mathbf{A}$.

$$\mathbf{A} = \begin{bmatrix} | & & | \\ u_1 & \dots & u_m \\ | & & | \end{bmatrix} \begin{bmatrix} \sigma_1 & & \\ & \ddots & \\ & & \sigma_m \end{bmatrix} \begin{bmatrix} — & v_1^T & — \\ & \vdots & \\ — & v_m^T & — \end{bmatrix} \tag{2.2}$$

There always exists the SVD for a real matrix, but the decomposition is not unique: if $\mathbf{A} = \mathbf{U}_1\Sigma\mathbf{V}_1^T = \mathbf{U}_2\Sigma\mathbf{V}_2^T$ then $\Sigma_1 = \Sigma_2$ but $\mathbf{U}_1 = \mathbf{U}_2\mathbf{B}_a$ and $\mathbf{V}_1 = \mathbf{V}_2\mathbf{B}_b$ for some block diagonal unitary matrices $\mathbf{B}_a, \mathbf{B}_b$ [17, 18]. Each column in $\mathbf{U}$ and $\mathbf{V}$ is an eigenvector of $\mathbf{A}\mathbf{A}^T$ and $\mathbf{A}^T\mathbf{A}$.

2.3.3 Principal Component Analysis

Principal Component Analysis is a staple of linear dimensionality-reduction techniques. The standard PCA procedure takes as input a matrix $\mathbf{B}$ representing n columns of data with m dimensions. The matrix is first mean-centered: $\mathbf{A}_{ij} = (\mathbf{B}_{ij} - \mu_i)$ where μ_i is the mean of the row i. The output of PCA is a set of vectors that explain most of the variance within $\mathbf{B}$. Given the covariance of the mean-centered matrix $\mathbf{A}$ is defined as $\mathbf{A}\mathbf{A}^T$, the Principal Components (PCs) maximise the following equation:

$$\text{Var}_i = \max_{\substack{x_i \in \mathbb{R}^m \setminus \{\mathbf{0}\} \\ \|x_i\|=1 \\ x_i \perp x_1 \dots x_{i-1}}} x_i^T \mathbf{A}\mathbf{A}^T x_i \tag{2.3}$$

As $\mathbf{A} = \mathbf{U}\Sigma\mathbf{V}^T$ from SVD, $\mathbf{A}\mathbf{A}^T = \mathbf{U}\Sigma\mathbf{V}^T\mathbf{V}\Sigma\mathbf{U}^T = \mathbf{U}\Sigma^2\mathbf{U}^T$. Therefore, it can be shown that the PCs $x_i = u_i$ from $\mathbf{U}$. The pair $\mathbf{U}, \Sigma$ will also be referred to as a subspace as they provide sufficient information to describe the original $\mathbf{B}$ matrix.

2.3.4 Subspace-Merge

Subspace-Merge is used to merge two subspaces together. Given two subspaces $(\mathbf{U}_1, \Sigma_1)$ and $(\mathbf{U}_2, \Sigma_2)$ from $\mathbf{Y}_1$ and $\mathbf{Y}_2$ respectively, the subspace of $\mathbf{Y} = [\mathbf{Y}_1, \mathbf{Y}_2]$ is:

$$\mathbf{U}\Sigma = \text{SVD}([\mathbf{U}_1\Sigma_1, \mathbf{U}_2\Sigma_2]) \tag{2.4}$$

$[\mathbf{A}, \mathbf{B}]$ signifies the concatenation of two matrices with the same number of rows.

2.3.5 Incremental-SVD

Incremental-SVD allows Pronto to become a streaming algorithm with limited memory. It takes a stream of chunks $\mathbf{Y}_i$, such that $[\mathbf{Y}_1, \dots, \mathbf{Y}_l] = \mathbf{Y}$, and with each recieved chunk it performs Subspace-Merge to produce $\mathbf{U}_l, \Sigma_l$ where $\mathbf{Y} = \mathbf{U}_l\Sigma_l\mathbf{V}_l^T$

Algorithm 1 Incremental-SVD

Data: $\mathbf{Y} = [\mathbf{Y}_1, \dots, \mathbf{Y}_l]$
Result: $\mathbf{U}_l, \Sigma_l$ such that $\mathbf{Y} = \mathbf{U}\Sigma\mathbf{V}^T$
  $\mathbf{U}_1, \Sigma_1, \mathbf{V}_1^T = \text{SVD}(\mathbf{Y}_1)$
  for $i = 2$ to l **do**
    $\mathbf{U}_i, \Sigma_i, \mathbf{V}_i^T = \text{SVD}([\mathbf{U}_{i-1}\Sigma_{i-1}, \mathbf{Y}_i])$
  end for

If the shape of the batches of data is $m \times b$, the space complexity of Incremental-SVD is $\mathcal{O}(m^2 + mb)$ as only the latest version of $\mathbf{U}_i, \Sigma_i$ and $\mathbf{Y}_i$ are needed for each iteration.

2.3.6 FPCA and FSVD

FPCA combines the relationship between standard SVD and PCA with the Subspace-Merge operation, to calculate the PCs of the data $[\mathbf{Y}_1, \ldots, \mathbf{Y}_m]$ from m nodes. Every node i performs perform SVD on their local data, to produce the subspace $\mathbf{U}_i, \Sigma_i$. These subspaces can be merged using at most $m-1$ Subspace-Merges to obtain the global subspace $\mathbf{U}'\Sigma'$, corresponding to the PCs of the aggregated data from all the nodes. PRONTO turns this procedure into a streaming algorithm, by running Subspace-Merge on the subspaces produced by incremental-SVD. Finally, PRONTO also introduces a forgetting factor γ in front of $\mathbf{U}_i\Sigma_i$ in Incremental-SVD that allows it to "forget" old data by gradually reducing the influence of previous subspaces. Like with standard PCA, FPCA can be considered as FSVD on mean-centered data.

2.3.7 Low-Rank Approximations

It can be shown that using the first r eignenvectors in the above algorithms approximate the result of using all m eignenvectors, i.e. if

$$\mathbf{Y} = \begin{bmatrix} | & & | \\ u_1 & \ldots & u_m \\ | & & | \end{bmatrix} \begin{bmatrix} \sigma_1 & & \\ & \ddots & \\ & & \sigma_m \end{bmatrix} \begin{bmatrix} — & v_1^T & — \\ & \vdots & \\ — & v_m^T & — \end{bmatrix} \tag{2.5}$$

We can use $\mathbf{U}^r = \begin{bmatrix} | & & | \\ u_1 & \ldots & u_r \\ | & & | \end{bmatrix}$ and $\mathbf{\Sigma}^r = \begin{bmatrix} \sigma_1 & & \\ & \ddots & \\ & & \sigma_r \end{bmatrix}$ where $r \leq m$ in Incremental-SVD and Subspace-Merge. This lets PRONTO reduce the number of computations it performs and its memory usage.

2.3.8 Pronto System Overview

There are two types of nodes in PRONTO: compute node (C) and aggregator node (A). Compute nodes collect and center node statistics (i.e. CPU and Memory) and perform Incremental-SVD to obtain the low rank approximations of the local subspace $\mathbf{U}, \Sigma$. The aggregator nodes perform Subspace-Merge on incoming subspaces, with subspace produced by the root aggregator node being propagated back to the compute nodes.

2.3.9 Pronto Reject-Job Signal

Each compute node projects their data onto the latest version of $\mathbf{U}$, and identifies all the spikes. If the weighted sum of these spikes, using the corresponding singular values in Σ, exceeds a threshold, a rejection signal is raised to indicate that the node is potentially experiencing performance degradation and a job should not be scheduled on that node.

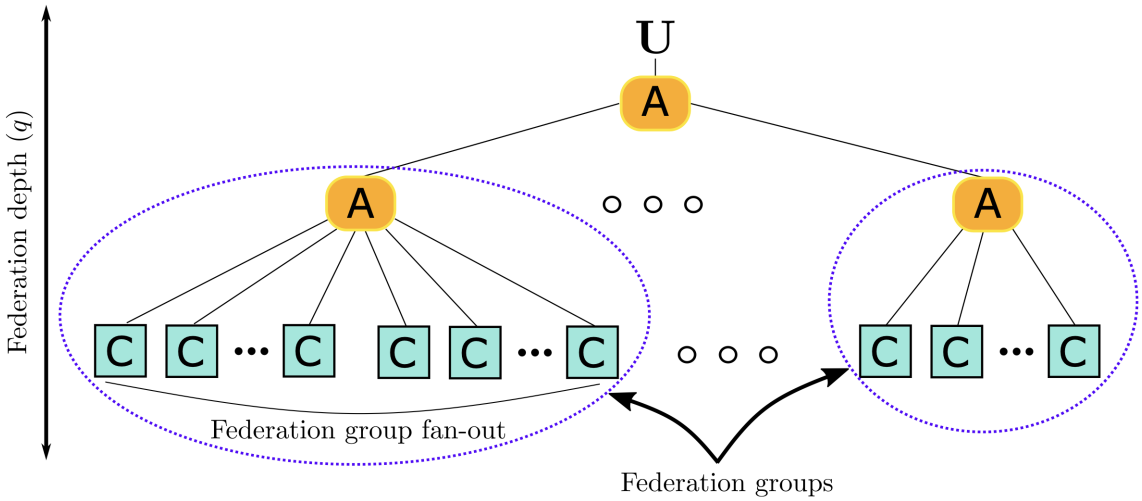

Figure 2.2: How local models are aggregated in PRONTO. Dedicated aggregator nodes propagate the updated subspaces until the root is reached [14].

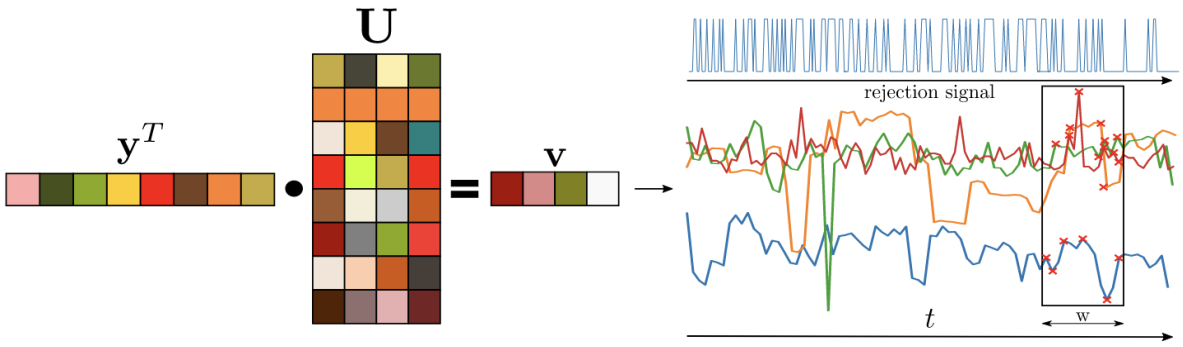

Figure 2.3: Projection of incoming $y \in \mathbb{R}^d$ onto embedding $U \in \mathbb{R}^{d \times r}$ producing R projections in $v \in \mathbb{R}^{1 \times r}$. Projections are tracked over time for detecting spikes which form the basis of the rejection signal. The sliding window for spike detection for each projection is of size w also shown in the figure.

2.3.10 Strengths

PRONTO's core strength is its ability to leverage global telemetry data to predict performance degradation with high accuracy. The orginal PRONTO paper [14], which compared its effectiveness against non-distributed dimensionality-reduction methods, demonstrated superior performance in predicting CPU-Ready spikes in real-world datacenter traces. This improved accuracy over the non-distributed strategies suggests that significant correlations exist between the resource usages of different jobs across various nodes at the same point in time. This federated approach allows for a more comprehensive understanding of system-wide resource contention, providing more accurate contention predictions than with only individual node data. These compelling results indicate a strong potential benefit from applying PRONTO underlying principles to a Kubernetes environment where

efficient resource management is paramount.

2.3.11 Weaknesses

While PRONTO offers a promising approach to performance prediction, its direct application within Kubernetes scheduling environment faces significant challenges due to fundamental assumptions and practical limitations of its original design.

Assumptions

The PRONTO paper primarily focuses on a method for measuring node "responsiveness" to future workloads, yielding a binary Reject-Job signal. However, implementing its design in a complex system like Kubernetes raises fundamental challenges:

1. **Zero-Latency Assumption:** A critical assumption in the PRONTO paper is the absence of communication latency, and implicitly binding latency within the system. This implies that scheduled workloads are immediately reflected in the telemetry, and thus the signal. In such a scenario, a central scheduler could instantaneously stop assigning workloads once a Node signal potential degredation. However, this assumption does not hold in real-world Kubernetes clusters. The latency between a pod being bound to a Node and that Pod actually starting to run and consume resources has been shown to reach as high as 4 seconds [15]. Directly applying PRONTO's binary signal in this high-latency environment could lead to a "runaway train" schenario": Nodes might advertise willingness to accept new Pods while a large number of "inflight" Pods are still pending startup and will overload the node once active.

2. **Lack of Explicit Allocation Algorithm:** PRONTO allows individual compute nodes to reject or accept incoming jobs. However, it does not explicitly provide a system to optimally decide which compute nodes are considered for a task. While a simple approach would be to allow individual Nodes to request Pending Pods, it suffers from scalability issues as hundreds of Nodes sending requests to the Kubernetes APIServer would greatly degrade its performance or even cause it to crash. Instead, I decided to take a centralised approach, where Nodes periodically update their signal to influence where Pods are allocated.

3. **Limited Scoring Capability:** Unlike typical Kubernetes schedulers that employ a scoring-function to rank Nodes and select the "optimal" fit [10], a binary signal offers no mechanism to differentiate between suitable Nodes. This could lead to suboptimal allocation decisions, potentially reducing overall cluster throughput and efficiency

These issues raise the need for a more sophisticated signal that is:

1. **Comparable:** provides enough information to score and rank Nodes effectively.

2. **Reservable:** allows the scheduler to track the pending impact of previous scheduling decisions until Pods have begin running.

Peak-Prediction

PRONTO relies on peak-detection within contention metrics (originally CPU-Ready in VMware vSphere) to predict future performance degradation. For PRONTO to generate an accurate Reject-Job signal in Kubernetes, the chosen contention metrics should exhibit clear, distinguishable spikes during genuine high-resource contention. While increasing the number of collected metrics can help reduce the impact of erroneous spikes, collecting more telemetry and operating on larger matrices will incur additional overheads and reduce the number of tasks a Node can accept before valid contention is detected.

Linux-based systems offer Pressure Stall Information (PSI) metrics, accessible via `/proc/pressure/<cpu`. These pseudo-files track the time tasks are stalled waiting for resources. To investigate the feasibility of using PSI for peak prediction within a Kubernetes Node, I polled the polled the `/proc/pressure` files under different workloads.

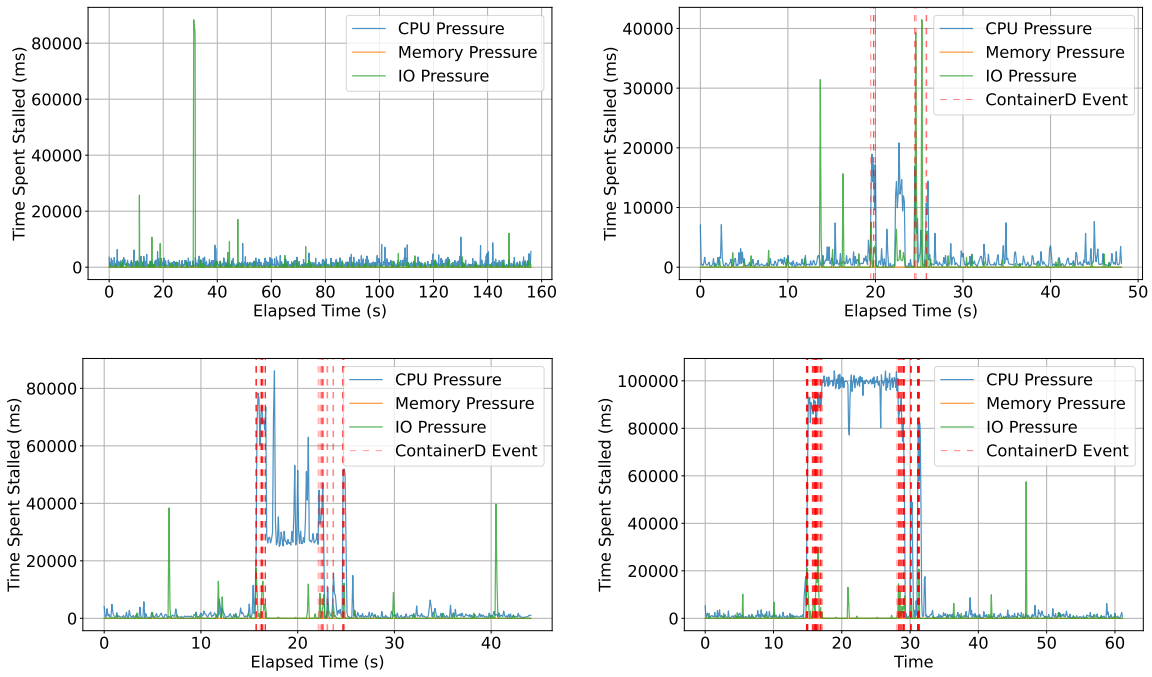

Figure 2.4: Measurements of `total` from `/proc/pressure/` under different loads. The container runtime results in spikes no matter the workload.

As demonstrated in Figure 2.4, even with lightweight workloads, the PSI metrics frequently experience significant spikes. These transient spikes can be attributed to the container runtime (e.g. Containerd) consuming resources during the creation or deleteion of containers. These "noise" would be difficult to distinguish from genuine indicators of resource contention , compromising the accuracy of PRONTO's peak-detection mechanism.

The PSI metrics also expose an average over a 10-second window. Figure 2.5 illustrates

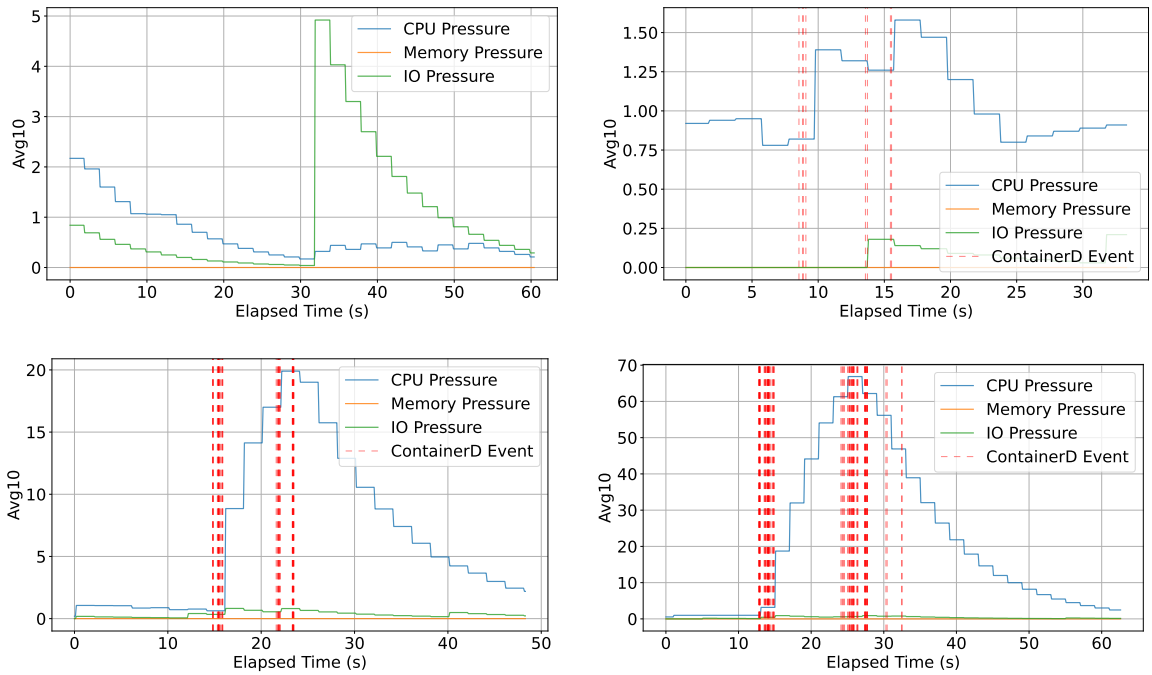

Figure 2.5: Measurements of `avg10` from `/proc/pressure/` under different loads. The container runtime results in spikes no matter the workload.

that averaging the PSI metrics can indeed reduce the impact of these container runtime-induced spikes. However, this smoothing comes at the cost of responsiveness. In the experiments with a 10-pod batch, the averaged metrics failed to converge on the true value observed in Figure 2.4 before the Pods had finished running. 10 seconds in the timeframe of Kubernetes can result in the same "runaway train" situation described earlier.

Based on this early empirical investigation, I conclude that direct peak-prediction from sub-second polling of raw PSI metrics, can not be easily applied within a fast-paced Kubernetes environment.

2.4 Related Work

This section examines existing Kubernetes schedulers, highlighting those that share characteristics with Pronto: distributed and federated schedulers, online schedulers, performance-aware schedulers, and machine learning-based schedulers.

2.4.1 Federated and Distributed Scheduling

Pronto is described as a federated algorithm that executes plans in a decentralised fashion. Each computing node makes independent decisions for task assignments without needing global synchronisation. This contrasts with monolithic centralised schedulers [10, 19], such as the default Kubernetes scheduler (`kube-scheduler`), which acts as a single dispatcher on the master node and has a global state view. These schedulers can

suffer from scalability issues, reliance on cached data and increased network traffic [14]. Research has been done in multi-cluster scheduling and cluster federation, addressing challenges in scalability and geo-distributed environments. Examples include frameworks like KubeFed [20] and architectural proposals like Foggy [21]. Although PRONTO immediate focus is on scheudling within a network of nodes that might not be geographically dispersed or owned by different entities, its federated learning approach to sharing knowledge through aggregated iterates is relevant to discussions around decentralised control and coordination in distributed infrastructures.

2.4.2 Performance-Aware and Predictive Scheduling

As a performance-aware scheduler, PRONTO employs dimensionality-reduction technique to efficiently process the vast amount of telemetry data produced by each node, with the goal of predicting performance degradation. While, CPU and RAM utilisation are common metrics for performance-aware Kubernetes schedulers [11, 22–25], PRONTO distinguishes itself as the first scheduler to incorporate CPU-Ready for task scheduling.

Furthermore, the dynamic nature of Kubernetes workloads strongly suggest that predictive techniques could improve scheduling efficiency and resource utilisation [26]. Traditional forecasting methods (such as exponential smoothing, ARIMA, and SVM) were also explored in [14] for CPU Ready spike prediction, but were found to have worse accuracy. This still remains an open research topic.

2.4.3 Machine Learning-Based Schedulers

PRONTO exploits unsupervised learning technique, specifically Federated PCA, to discover hidden correlations within unstructured high-dimensional telemetry data. Machine Learning (ML) algorithms are increasingly adopted in scheduling to learn from data and improving decision quality. Reinforcement learning-based schedulers [11, 12, 27, 28] use reward functions to continuously improve scheduling decisions. While, ML has been used before to predict application or resource utilisation [13, 24, 29], these schedulers are typically domain-specific. PRONTO's application of unsupervised PCA to predict the performance of a Node represents a novel use-case of ML with broad applications within the scheduling domain.

2.4.4 Summary of Related Work

In summary, PRONTO distinguishes itself within the Kubernetes scheduling landscape through its federated and decentralised approach, enabling independent decision-making at the node level. Its streaming algorithm allows for immediate, low-latency task assignments. As a performance-aware scheduler, it innovatively uses CPU-Ready for task scheduling and applies unsupervised Federated PCA for predictive insights, offering a

distinct machine learning approach.

2.5 Summary

This chapter provided the foundational knowledge for the dissertation, introducing an overview of the Kubernetes architecture and its scheduling mechnaism. It then introduced Pronto, a novel approach to scheduling, explaining the core mathematics behind its FPCA, and highlighting its accuracy in predicting performance degradation through global telemetry. However, significant weaknesses were identified, emphasising the necessity for a more sophisticated **comparable** and **reservable** signal. Finally, a review of existing Kubernetes schedulers, helped distinguish **Pronto** from the current landscape and highlight it potential contribution.

Chapter 3

Carico

This chapter details CARICO, a federated, asynchronous, memory-limited algorithm, building upon the principles of PRONTO. CARICO differentiates itself from PRONTO for the following reasons:

1. Rather than performing standard FPCA, CARICO applies FSVD on non-centered observed resource usage. Subsequently, CARICO uses new interpretations for the results of SVD and presents a modification of the Subspace-Merge to preserve the interpretations.

2. CARICO presents a novel continuous and **comparable** capacity signal function that combines the new model interpretations with a Node's current resource usage to calculate the estimated workload capacity.

3. CARICO makes two assumptions to translate the calculated capacity signal into a signal that is both **reservable** and uses the number of Pods as its unit of measure.

As this algorithm produces a signal that measures "capacity", I will refer to it as CARICO - "load" in Italian.

3.1 Capacity Signal

In Section 2.3.11, we identified critical limitations of PRONTO's binary "Reject-Job" signal within the Kubernetes ecosystem: its lack of comparable Node scoring and inability to handle Pod startup latencies. While one could conceivably compare the number of detected spikes, this does not translate into a reservable signal, meaning it's impossible to quantitatively assign or reserve "peak detections" for incoming Pods. Furthermore, as will be shown empirically in Figure 4.4, contention metrics often do not change proportionally to the number of tasks assigned, making them difficult to reserve accurately.

To overcome these limitations, a signal reflecting varying levels of contention and offering a predictable, scalar relationship with task assignments was necessary. This led us to re-

consider a metric of capacity. Supported by its use within `kube-scheduler`, this approach provides the necessary properties to make it compatible with reservation mechanisms. To produce a measure of capacity, we had to deviate from FPCA as its interpretations focused on the variability within telemetry data rather than its magnitude. The subsequent challenge was to find a means of transforming PRONTO's mathematical framework to produce values that could be interpreted as the direction and magnitude of recent workload's resource usage. Only once we had this interpretation, could we then develop a continuous, comparable, and reservable signal that could effectively and accurately guide scheduling decisions.

3.2 Local Model

In PRONTO, each individual compute node builds a local model of its resource usage by performing Incremental-SVD on incoming batches of mean-centered telemetry data and its latest local model. The resulting $\mathbf{U}$ can be interpreted as the PCs of the original telemetric data, and the singular values in Σ can be used to weight the different PC projections accordingly.

CARICO assumes that the telemetric data collected by Nodes is [0,1]-normalised. A batch of telemetric data $\mathbf{A}$ is an $m \times n$ matrix, where $\mathbf{A}$ contains n samples of m-dimensional columns of data. Each dimension in the vector represents a different resource, where the value 0 indicates that full capacity is available for that resource and 1 indicates that the resource is being fully used. This means results in $\mathbf{A}$ being non-negative with $0 \leq a_{ij} \leq 1$ for all i, j. As we are no longer mean-centering the dataset before applying SVD, **PCA's interpretations no longer apply to the resulting U and Σ matrices**.

Instead, CARICO is built on top of a different set of interpretations. Using the Lemma proved in Appendix A.1, we can interpret the first left singular vector u_1 in $\mathbf{U}$ as a pseudo-weighted average direction of the datapoints in the matrix: "larger" or more aligned columns contribute more significantly to the sum defining u_1, and thus to its final direction. CARICO, thus uses u_1 as a primary indicator of the direction of the current workload's resource usage.

While knowing the proportion of resource usage is useful, it is also important to be able to differentiate between lightweight workloads and more intense workloads. For this, CARICO uses the first singular value σ_1 in Σ. Given $\sigma_1(\mathbf{M})$ and u_1 correspond to the first singular value and first left singular vector of the non-negative matrix $\mathbf{M}$, the following holds:

$$\sigma_1(\mathbf{M})^2 = u_1^T \mathbf{M}\mathbf{M}^T u_1 \tag{3.1}$$

$$= (u_1^T \mathbf{M})^2 \tag{3.2}$$

Given m_j is the j-th column of $\mathbf{M}$, $\sigma_1(\mathbf{M})^2$ can be interpreted as the sum of squared scalar projections of columns in $\mathbf{M}$: $\sigma_1(\mathbf{M})^2 = \sum_{j=1}^{n}(u^T m_j)^2$.

Furthermore, the first singular value can be shown to scale with resource usage. Given two batches of telemetry $\mathbf{A}$ and $\mathbf{B}$ where batch $\mathbf{B}$ experienced more resource usage ($0 \leq a_{ij} \leq b_{ij} \leq 1$ for all i, j), it is shown in Appendix A.2 that the first singular value of $\mathbf{B}$ will be greater than or equal to that of $\mathbf{A}$ ($\sigma_1(\mathbf{A}) \leq \sigma_1(\mathbf{B})$. With these properties, the first singular value makes a good indicator of measured resource usage.

3.3 Subspace Merging

While we have shown that the results from performing SVD on [0,1]-normalised telemetry data can have useful interpretations, the resulting σ_1 can grow with each Incremental-SVD:
Given two non-negative matrices $\mathbf{A} \in \mathbb{R}^{m \times n_1}$ and $\mathbf{B} \in \mathbb{R}^{m \times n_2}$, the first singular value of the concatenated matrix $\mathbf{C} = [\mathbf{A}, \mathbf{B}]$ is greater than or equal to the maximum of the first singular values of $\mathbf{A}$ and $\mathbf{B}$. That is,

$$\sigma_1([\mathbf{A}, \mathbf{B}]) \geq \max(\sigma_1(\mathbf{A}), \sigma_1(\mathbf{B}))$$

This is proved in Appendix A.3.

This property is important, as we established earlier that σ_1 is used by CARICO as an indicator of the magnitude of resource usage. If σ_1 can increase while the measured telemetry reports a stable magnitude of resource usage, its interpretation no longer holds.

A solution is to scale the concatenated matrices using non-negative scalar weights $\gamma_{\mathbf{A}} = \sqrt{w_{\mathbf{A}}}$ and $\gamma_{\mathbf{B}} = \sqrt{w_{\mathbf{B}}}$ such that $w_{\mathbf{A}} + w_{\mathbf{B}} = 1$. This method still preserves the earlier interpretations:

- **First Left Singular Vector:**
  The resulting first singular vector u_1 of the concatenated matrix $\mathbf{C} = [\gamma_{\mathbf{A}}\mathbf{A}, \gamma_{\mathbf{B}}\mathbf{B}]$ still behaves as a pseudo-weighted average, but with the contributions of the input telemetry further weighted according to the scalar weights. This is useful as using different values for $\gamma_{\mathbf{A}}$ and $\gamma_{\mathbf{B}}$ behaves similarly as the forget factor γ used in PRONTO.

- **First Singular Value:**
  In addition, Appendix A.4 proves that the resulting first singular value and the first left singular vector of the concatenated matrix $\mathbf{C} = [\gamma_{\mathbf{A}}\mathbf{A}, \gamma_{\mathbf{B}}\mathbf{B}]$ has the following property:

$$\min(P_{\mathbf{A}}(u_{\mathbf{C}}), P_{\mathbf{B}}(u_{\mathbf{C}})) \leq \sigma_1(\mathbf{C})^2 \leq \max(P_{\mathbf{A}}(u_{\mathbf{C}}), P_{\mathbf{B}}(u_{\mathbf{C}}))$$

where $\sigma_{\mathbf{C}}$ and $u_{\mathbf{C}}$ correspond to the first singular value and first left singular vector of $\mathbf{C}$, $P_{\mathbf{M}}(u)$ is the sum of squared scalar projections of the columns in $\mathbf{M}$ onto u (let m_j be the j-th column of $\mathbf{M}$ $P_{\mathbf{M}}(u) = \sum_{j=1}^{n}(u^T m_j)^2$). As $\sigma_1(\mathbf{C})^2$ is a convex combination of $P_{\mathbf{A}}(u_{\mathbf{C}})$ and $P_{\mathbf{B}}(u_{\mathbf{C}})$, it is effectively a weighted mean of these two projected sums and ensures σ_1 reflects the magnitude of the observed resource usage.

3.4 Capacity Signal Function

Using the interpretations established above:

- u_1: the pseudo-weighted average direction of resource usage of recent workloads
- σ_1: the magnitude of the resource usage of recent workloads

we can calculate a new capacity signal that considers both the estimated workload resource usage and its current resource usage. Given the the current [0,1]-normalised resource usage vector for the node y, the first singular value and left singular vector σ_1, u_1 from the latest U and Σ, a Node's estimated capacity signal k is given by:

$$y_{\text{predict}} = y + k * \sigma_1 u_1 \tag{3.3}$$

$$\max_k \forall i : y_{\text{predict}} < 1 \tag{3.4}$$

The resulting k represents how many "units" of the learned "average" workload ($\sigma_1 u_1$) can be added to the current workload (y) before any single resource dimension hits its normalised capacity of 1. In the following sections, I will refer to k as "Capacity".

3.4.1 Example Scenarios

To better understand how this signal works, I will explore how the signal changes under different different loads. This scenarios will also be used to control the correctness of the signal implementation in the prototype.

Figure 3.1 presents the scenario where a Node updates its local model, learning that the experienced workload has increased in resource usage (σ_1 has increased). This means that a smaller constant k is needed before the combined vectors cross a resource boundary. As a result, a Node advertises a smaller capacity signal as it has less capacity for the expected resource usage.

Figure 3.2 presents the scenario where a Node updates its local model, learning that the learned workload is using more resources but in a different direction. This could be described as a complementary workload as the the dot product of the current resource utilisation and the expected resource utilisation is much smaller. Therefore, a larger constant k is needed to cross a resource boundary. This results in a Node advertising a higher capacity signal as it has more capacity for the new expected resource utilisation.

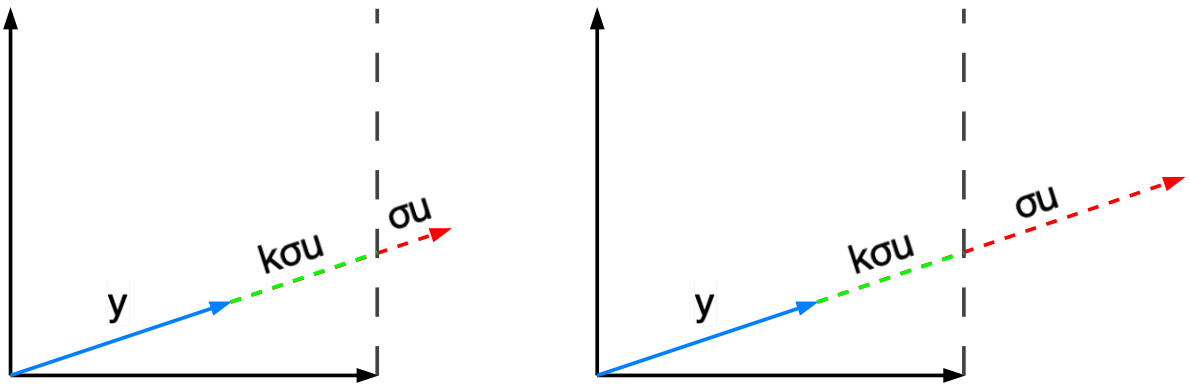

Figure 3.1: Visualisations of a Node's resource usage y and expected resource usage $\sigma_1 u_1$ when learning of conflicting resource utilisation.

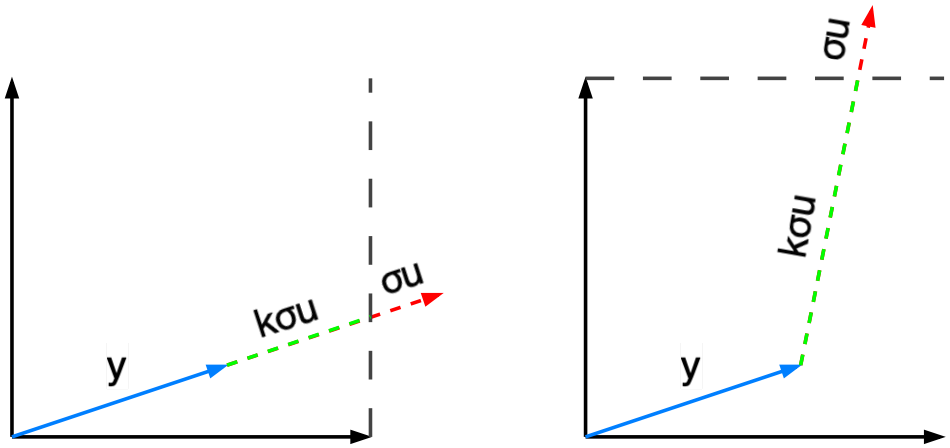

Figure 3.2: Visualisations of a Node's resource usage y and expected resource usage $\sigma_1 u_1$ when learning of complementary resource utilisation.

3.5 Reserve Cost and Capacity

Like Pronto, Carico's signal uses its current resource usage, and therefore, only reflects Pods that have been scheduled and are running on the Node. For Carico to work in a system with Pod startup latency, the scheduler must be able to predict the effect a Pod will have on a Node's signal. Carico assumes that Nodes know the number of currently running Pods, as well as, have the ability to estimate their:

1. **Baseline Capacity Signal:** the Capacity signal when no Pods are running

2. **Per-Pod-Cost:** the estimated amount that the Capacity signal will drop when a single Pod starts running.

Section 4.2.4 implements and compares different prediction methods. With this information, a Node can calculate its Pod-Capacity from:

$$\text{Pod-Capacity} = \frac{\text{Current Capacity Signal}}{\text{Per-Pod-Cost}} \tag{3.5}$$

$$\text{Pod-Capacity} = \frac{\text{Baseline Capacity Signal}}{\text{Per-Pod-Cost}} - \text{Current Pod Count} \tag{3.6}$$

This metric has two useful properties:

- **Dual-Mode:** Pod-Capacity can be calculated using two equations. This is especially useful in Kubernetes as during the creation or deletion of a Pod, the measured resource usage can experience large spikes. While filtering can mitigate these spikes, they are still observable in Figure 4.5. To combat this noise, Nodes can switch to predicting Pod-Capacity using estimated capacity and Pod count. This reduces fluctuations in a Node's advertised capacity and improves scheduling decisions
- **Unit of Measure:** Pod-Capacity's unit of measure is in terms the number of Pods. This simplifies the central scheduler's logic as it does not need to keep track of each Node's Per-Pod-Cost.

Each Node n will broadcast its Pod-Capacity$_n$ to a central scheduler. This scheduler also tracks each Node's reserved amount as # Pods Reserved$_n$. For each Pod waiting to be assigned to a Node, the scheduler performs the following operations:

- **Filter:** Filters out all Nodes n with Pod-Capacity$_n$ − # Pods Reserved$_n$ < 1. Ensures we do not schedule on Nodes that do not have enough resources for another pod. While we could reduce the limit to improve throughput by packing more Pods on a Node, it could result in OOM kills if there isn't enough memory available on a Node for all of the Pods.
- **Score:** Score Nodes n by Pod-Capacity$_n$ − # Pods Reserved$_n$. This ensures we allocate to Nodes which can fit more Pods.
- **Reserve:** Once a node is Node has been chosen, we increment # Pods Reserved$_n$ by 1 for that Node. Once a scheduled Pod is no no longer in the Pending state, the central scheduler decrements # Pods Reserved$_n$ by 1 for the Node n the Pod was assigned to.

3.6 Properties

PRONTO is designed to be *federated, streaming* and *unsupervised*. CARICO exhibits identical properties while also considering the existance of communication and Pod startup latency.

Federated: PRONTO executes scheduling plans in a decentralised fashion without knowl-

edge of the global performance dataset. Such approach in Kubernetes could actually decrease performance. The Kubernetes API server handles the publishing and updating of Kubernetes objects. A decentralised system with no global synchronisation or coordination could result in a stampede of Bind requests that could overload the Kubernetes API server and slow down the publishing of incoming Pods. Instead, CARICO uses a central scheduler to score Nodes and perform the final Bind operation. However, it can still be considered federated because of its use of federated SVD []: individual Nodes can have a unified view of the global workload while maintaining their individual autonomy to set their score as they deem fit.

Streaming: CARICO's use of Incremental-SVD, like PRONTO, means it only requires memory linear to the number of features considered; given batches of dimension $d \times b$, the required memory is proportional to $\mathcal{O}(d)$. As CARICO still works with low-rank approximations, its memory footprint can be reduced even further. Furthermore, like PRONTO, CARICO only requires a single pass over the incoming data without having to store historical data in order to update its estimates.

Unsupervised: CARICO uses FSVD and assumptions about the collected telemetry to generate values with capacity-based interpretations. While this greatly differs from PRONTO and its use of FPCA, CARICO still exploits the resulting subspace estimate along with the incoming data to reveal patterns in recent resource-usage.

Continuous Value PRONTO is a binary signal, which makes it difficult to score Nodes. CARICO's Pod-Capacity $\in \mathbb{R}$, allowing Nodes to be filtered and scored against each other.

Latency Resilient: Unlike PRONTO which assumes no communication latency, CARICO was designed with Kubernetes in mind, and thus must consider possible latency in communication and Pod startup. CARICO's Pod-Capacity's unit of measure allows the central scheduler to easily track the estimated cost of Pods in-flight, ensuring subsequent scheduling decisions do not mistakenly overload a Node with a high Pod-Capacity.

Chapter 4

Implementation

4.1 System Architecture

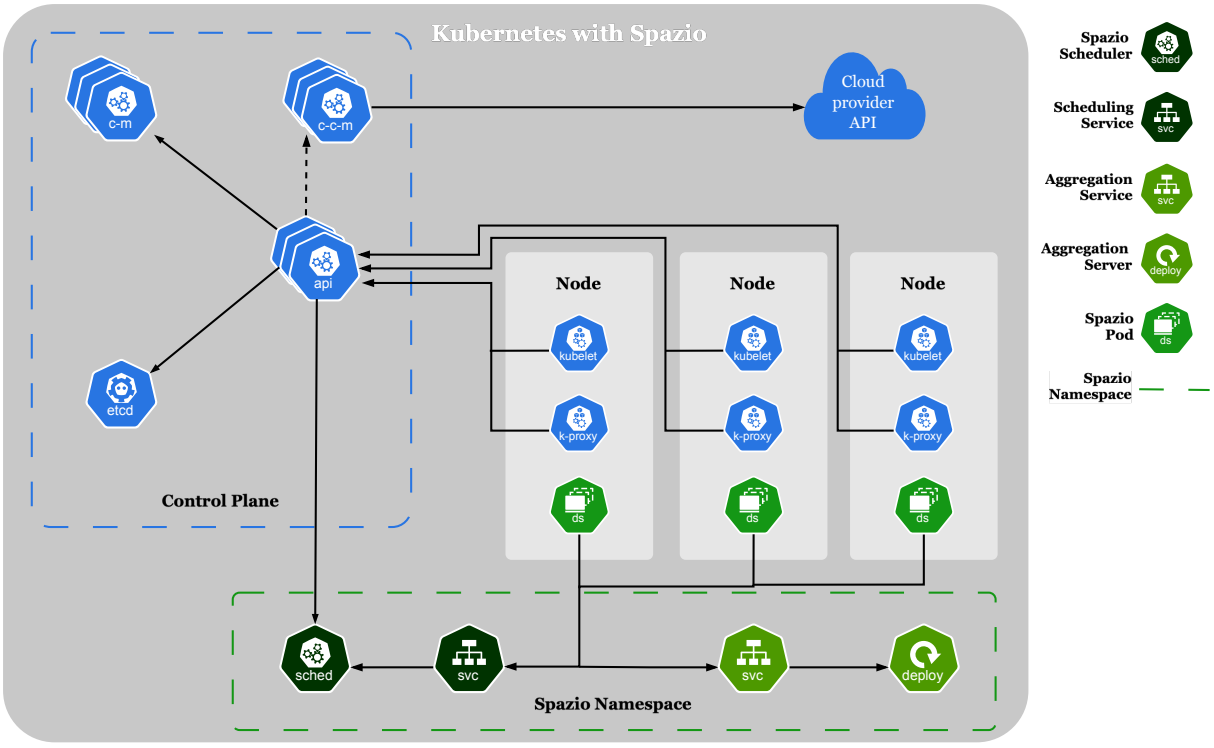

Figure 4.1: The components within the Carico system

The Carico system consists of three core components (shown in figure 4.1):

- Carico DaemonSet: each Node in the cluster will contain a Carico Pod. This Pod periodically collects telemetry from the Node and generates its local model and a capacity signal, which it sends to the Scheduling Service. When the Carico Pod deems its local model outdated, it requests the latest aggregated global model from the Aggregation service.

- Aggregation Server: This deployment provides the Aggregation service. The Aggregation Server Pod receives local models from Nodes and returns the latest aggregated global model.

- Scheduler: In CARICO, the scheduler is a **Scheduler Plugin**, implementing custom Filter, Score and Reserve functions. It also acts as the server of the Scheduling service, receiving the latest capacity scores of each Node to inform its scheduling decisions.

4.2 Carico Pod

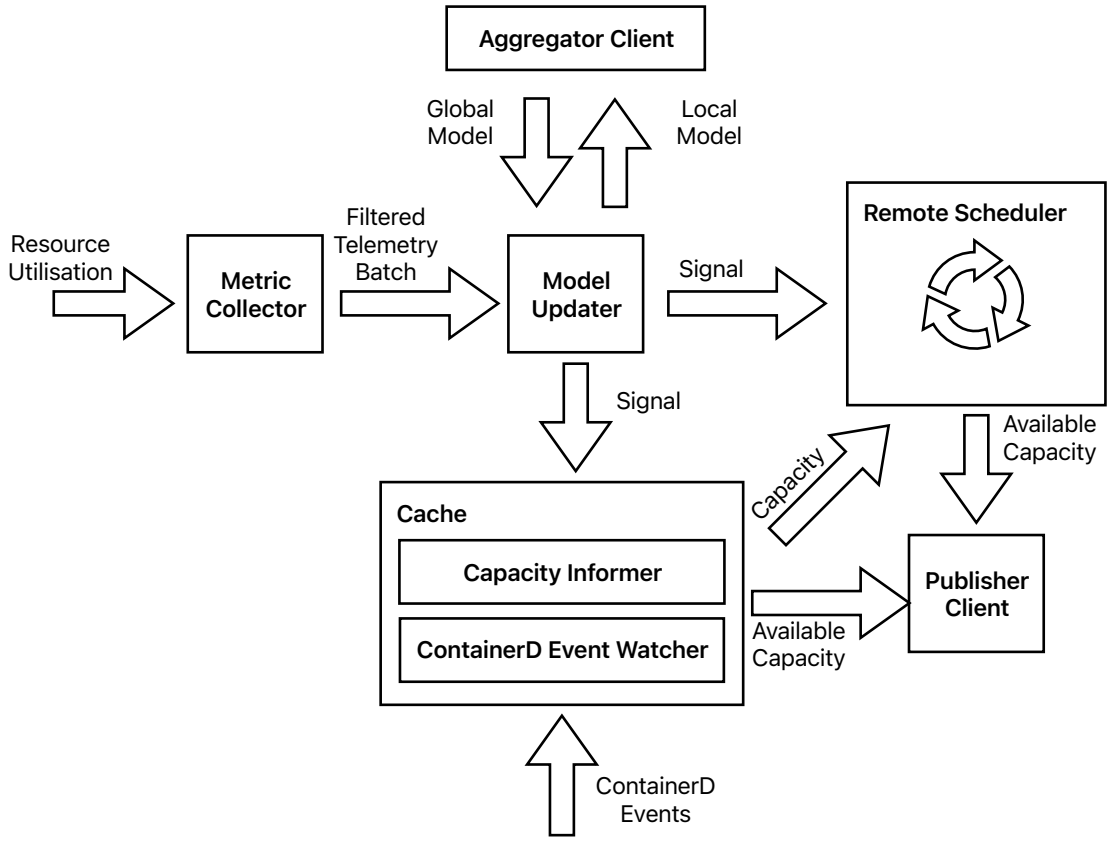

Figure 4.2: Core components within the CARICO Pod

As mentioned in section 4.1, the CARICO Pods are defined within a DaemonSet - a DaemonSet ensures that all Nodes run a copy of a Pod. The CARICO Pods collect telemetry from the Node and generate its local model and capacity signal. The following sections detail the metrics considered and explain the corresponding implementation decisions.

4.2.1 Metric Collection

To build its local model, the CARICO Pod must first collect telemetry. Kubernetes offers numerous ways to obtain telemetry data. I explored two primary sources of telemetry data:

- Metrics Server: a cluster add-on that acts as a centralised source of container reosurce metrics.
- `/proc/`: a pseudo-filesystem within Linux that exposes real-time information about running processes and system's hardware.

With Metrics Server, a scraper is used to periodically (default every 15 seconds) collects resource metrics from Kubelets and exposes them from its `metrics.k8s.io/v1` APIService. While simple to use, it offers limited metrics (CPU and RAM utilisation only) and introduces additional latency. Moreover, its default 15 seconds scraping interval is too infrequent, potentially missing short-lived Pods entirely.

`/proc/`, conversely, offers low latency access to an up-to-date view of the current state of the system. Furthermore, `/proc/` contains various files and subdirectories, each providing specific information. Examples include, `/proc/stat` which contains the amount of time CPU cores spend in different states, `/proc/meminfo` provides statistics about memory usage, `/proc/diskstats` presents the raw, low-level I/O statistics of all block devices. Finally, both these sources are not generated periodically, but rather on-the-fly. This guarantees that the information you see is as current as the system's internal state.

Given these advantages, I selected `/proc/` as the source of telemetry data. The subsequent sections detail the metrics I considered and their rationale behind their use.

Utilisation Metrics

`/proc/` can generate standard utilisation metrics (e.g., CPU and memory percentage usage). These metrics are widely used in industry [30, 31].

To collect CPU utilisation, I used the `/proc/stat` file. This file reports the cumulative count of "jiffies" (typically hundredths of a second) each CPU spent in a specific mode [32]. I can then calculate CPU utilisation using:

$$\text{CPU Usage\%} = 1 - \frac{\Delta\text{idle} + \Delta\text{iowait}}{\Delta\text{across all fields}}$$

`/proc/meminfo` can also be used to collect memory utilisations. This file shows a snapshot of the memory usage in kilobytes. The percentage of memory used can then be calculated from the given field:

$$\text{Memory Used\%} = 1 - \frac{\text{MemFree} + \text{Buffers} + \text{Cached}}{\text{MemTotal}}$$

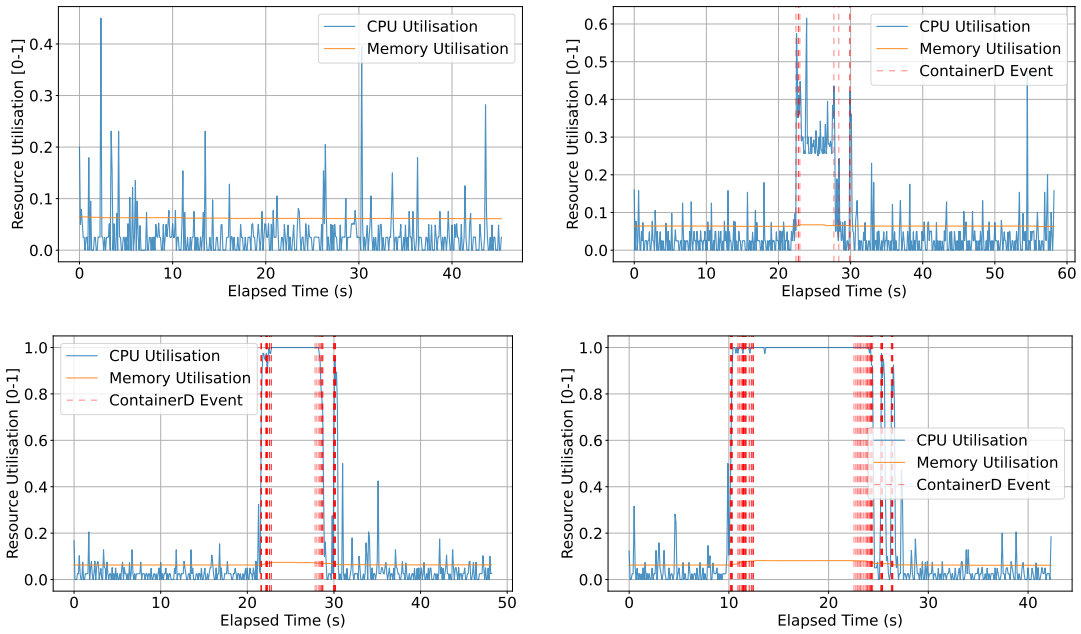

Figure 4.3: In this figure we sample CPU and memory utilisation from values of `/proc/stat`, `/proc/meminfo` at 10Hz during various Kubernetes workloads.

To assess their suitability for Carico, I measured utilisation metrics under various workloads. Figure 4.3 presents the metrics behaviour when running different Job sizes of `pi-2000` Pods. For a CPU-intense workload (calculating π to 2000 digits), the CPU utilisation correctly increased while memory utilisation remained stable.

Issues of using CPU Utilisation

Early prototypes using only utilisation metrics showed poor throughput compared to the default `kube-scheduler`, highlighting a problem with relying solely on CPU utilisation. When deploying 1000 Pods, each requesting 100 milliseconds of CPU time, across 19 Nodes, the `kube-scheduler` would immediately allocate all Pods evenly across the Nodes. This would result in $\approx$ 45 Pods running on each Node. In contrast, Carico (using only utilisation telemetry) allocated at most 5 Pods concurrently per Node. In both situations, CPU utilisation was 100%, however, the default `kube-scheduler` managed to achieve a high throughput, even with a long-tailed distribution of individual Pod completion times.

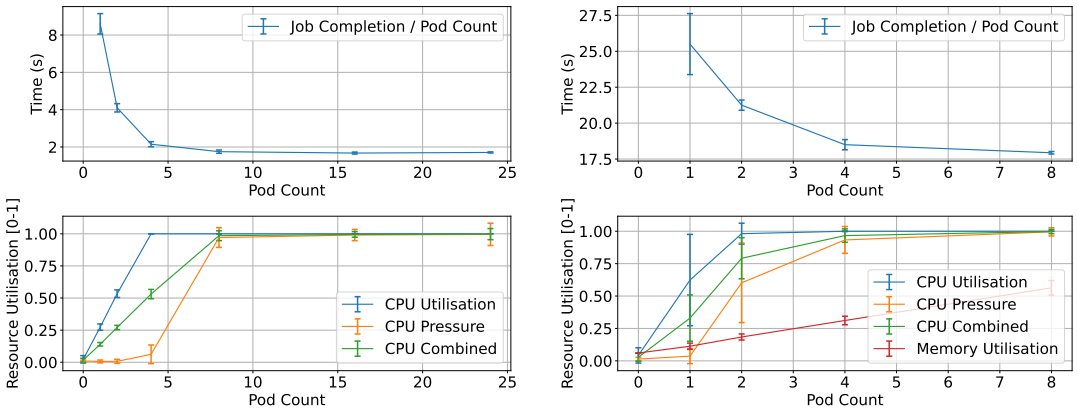

Figure 4.4: Collected resource metrics during various Kubernetes workload.

As a result, I decided to further investigate this phenomenon. Figure 4.4 shows how a Job's completion time changes as you increase its completion and parallelism count when running different Pods: cpu-intense Pi-2000 and a small ML workload (training and inference). I also decided to include measurements from `/proc/pressure`. This investigation revealed that the relationship between the number of Pods running on a Node at a time and their completion time showed a close-to linear relationship. I hypothesise that this is because the cluster runs on virtual machines (VMs). Hypervisors, while abstracting hardware, can mask effects like cache contention and CPU thrashing. This means that high CPU utilisation may not truly signify performance degradation. Thus, CPU utilisation alone is not a definitive capacity measure, explaining the prototype's initial throughput limitations.

Combining CPU Utilisation and CPU Pressure

Raw `/proc/pressure` metrics were also insuffice as these metrics barely increased until the Pod count exceeded core count. This would lead to unreasonably low intial Per-Pod-Cost estimations and an inflated advertised Node Pod-Capacity. I therefore combined both CPU utilisation and CPU pressure into a single metric:

$$CPU = \frac{\text{CPU Utilisation} + \text{CPU Pressure}}{2}$$

This ensures the metric increases with Pod count but doesn't saturate to quickly. This combined CPU metric only reaches its maximum when `/proc/pressure` indicates persistant CPU demand (at least one thread always waiting). Figure 4.4 illustrates this metric in action.

4.2.2 Filtering Metrics

Carico does not perform peak detection, but its signal is still susceptible to short-lived spikes. As previously noted, Pod creation and deletion incur visible resource usage spikes. These spikes introduce noise into both the Node's local model, as well as, its Capacity signal. A noisy signal complicates baseline Capacity and Per-Pod-Cost estimation. As such, I needed to de-noise the original metrics.

Investigation into the recorded telemetry showed that the spikes caused from container events would last ≈200 milliseconds. Sampling at 10Hz, Dynamic EMA was used to suppress container-event caused spikes (typically ≈ 200ms) while allowing rapid convergence for sustained changes (spikes > 300ms).

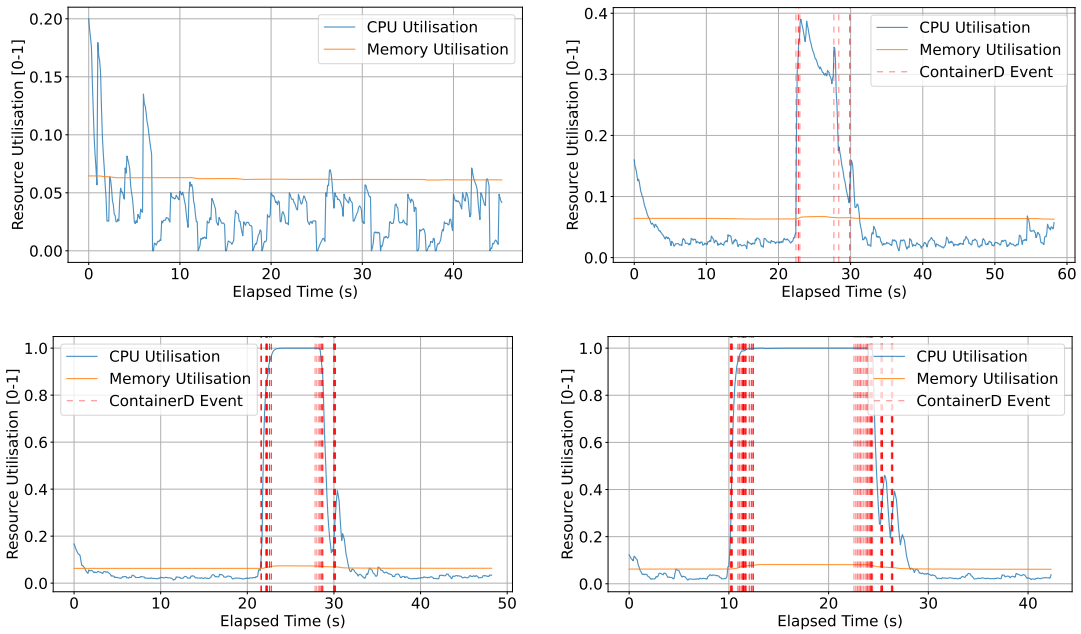

Figure 4.5: This figure shows the smoothed metrics under different workloads.

Comparing Figure 4.3 with 4.5 demonstrates the dampening of the Dynamic EMA and its quick responsive to prolonged changes in workloads. More sophisticated filters were avoided due to their higher computational cost, which would rob resources from scheduled Pods. Filtering the signal directly, rather than the telemetry, was considered but rejected as it would still allow container-event resource spikes to pollute the local model.

4.2.3 Signal Generation

The Carico Pod calculates its Capacity signal at 1Hz. This matches the local model update frequency, ensuring that the Capacity signal tracks with the local model. While a higher frequency would provide the central scheduler a more current view of a Node's resource status, it would also increase resource overhead. This overhead would reduce

the available resources to other Pods and could also lower the baseline Capacity signal, potentially reducing the capacity a Node advertises.

To verify Capacity signal's implementation, I tested it under the scenarios described in Section 3.4.1. For the conflicting workload, I had the measured Node execute a light CPU-focused workload (`ng-stress --cpu=8 --cpu-load=25`) with the surrounding Nodes executing a CPU-intense workload (`bpi(2000)`). For the complementary workload, the measured Node executed a light Memory-focused workload (`ng-stress --vm=4 --vm-bytes=4G`) with the surrounding Nodes also executing the same CPU-intense workload as in the conflicting scenario. The measured signals are shown in figures 4.6 and 4.7

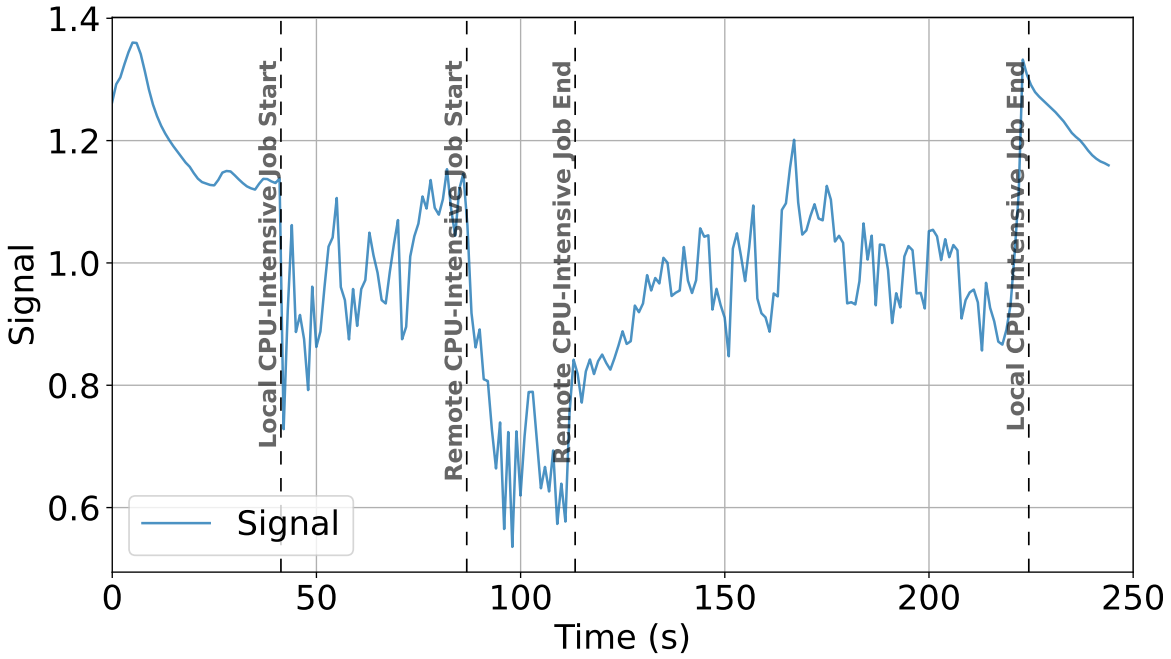

Figure 4.6: The calculated capacity signal of a Node running `ng-stress --cpu=8 --cpu-load=25`. While running this workload, 1000 Pods running `bpi(2000)` were scheduled across surrounding Nodes.

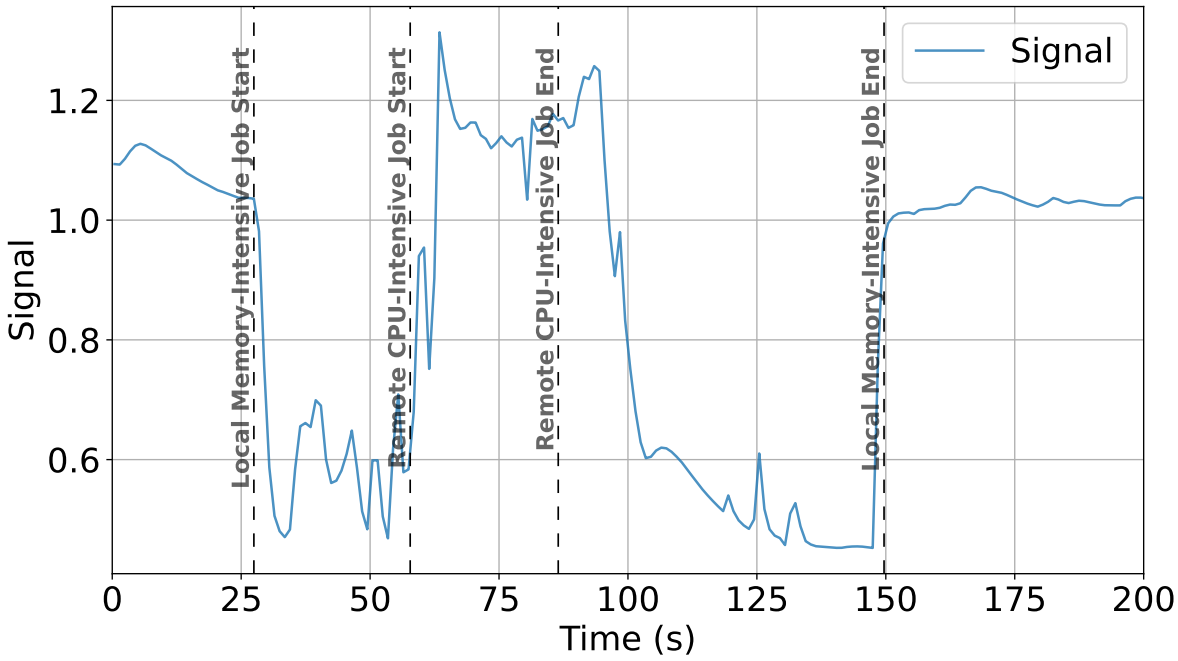

Figure 4.7: The calculated capacity signal of a Node running `ng-stress --vm=4 --vm-bytes=4G`. While running this workload, 1000 Pods running `bpi(2000)` was scheduled across surrounding Nodes.

Figures 4.6 and 4.7 demonstrates how a Node's capacity signal reacts to changes in surrounding workloads when experiencing different resource usage. In Figure 4.6, the measured Node is running a light CPU-focused workload. Once the CPU-intense workload is scheduled on surrounding Nodes, the measured Node's capacity signal drops. This is expected as the local models of surrounding Nodes will reflect a more costly CPU-focused workload. As a result, when the measured Node aggregates its local model, its new model will reflect this higher CPU usage with a larger σ_1 value. Since both the Node's current resource usageand the learned expected workload (reflected in u_1) are CPU-focused, the increased magnitude of the expected workload (larger σ_1) results in a smaller k (fewer units of this workload can be added), and thus a lower Capacity signal.

In Figure 4.7, the measured Node runs a light memory-focused workload. When the CPU-intense workload is scheduled on surrounding Nodes, the measured Node's capacity signal increases. This aligns with the hypothesis from Section 3.4. Like in the previous scenario, the global model reflects a heavy CPU-focused workload, and thus, so will the aggregated local model of the measured Node. However, with the Node's current resource usage (memory-focused) now largely orthogonal to the learned expected workload (CPU-focused), a larger k is required to reach a resource limit.

4.2.4 Calculating Cost and Capacity

Since the CARICO Capacity signal incorporates current resource usage, newly scheduling (but not yet running) Pods do not immediately affect the Capacity signal. Therefore, a signal reservation mechanism is needed to prevent the scheduler from greedily overloading the Node with the current highest score. To handle varying Pod workloads, a dynamic estimation of a Pod's "signal cost" was required. The method also needed to handle concurrent Pod creation and deletions.

Detecting Pod Events

There are numerous ways to detect the addition and removal of Pods from a Node. I investigated two event detection approaches: watching the Kubernetes API vs ContainerD events. The goals of the listeners were as follows:

- Detect the creation and deletion of Pods to establish a Pod count
- Provide warning for potential container-caused churn

This warning is crucial because the Dynamic EMA can't fully smooth prolonged resource spikes from multiple, concurrent container events. Early detection allows temporarily halting estimations during such bursts.

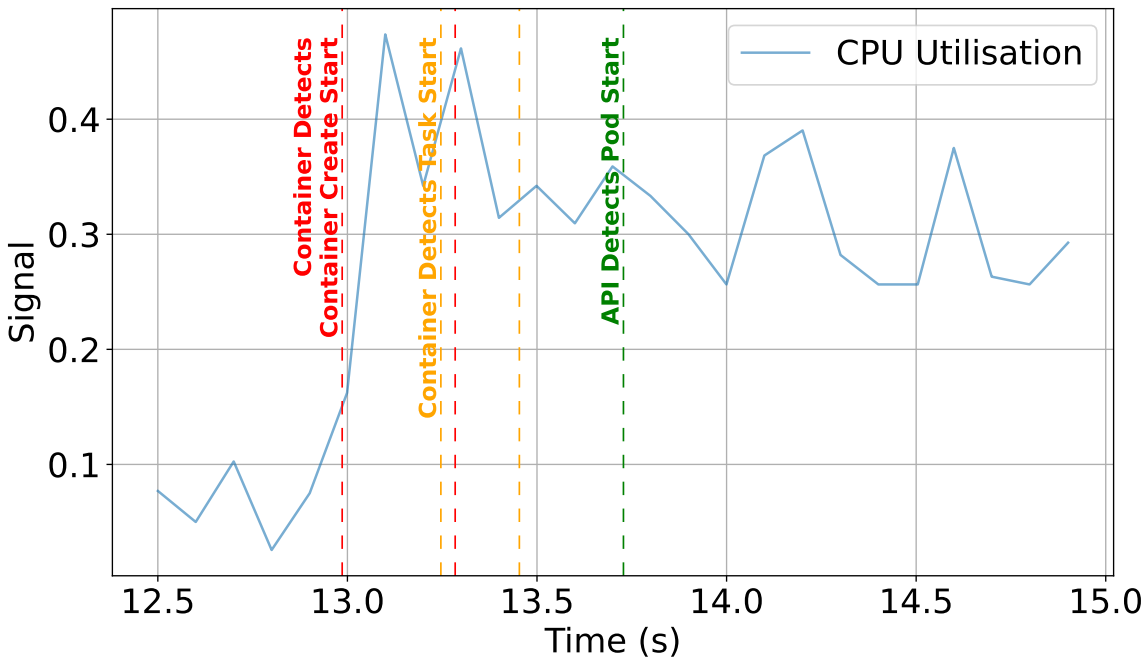

Figure 4.8: When different event listeners detected the creation of a Pod.

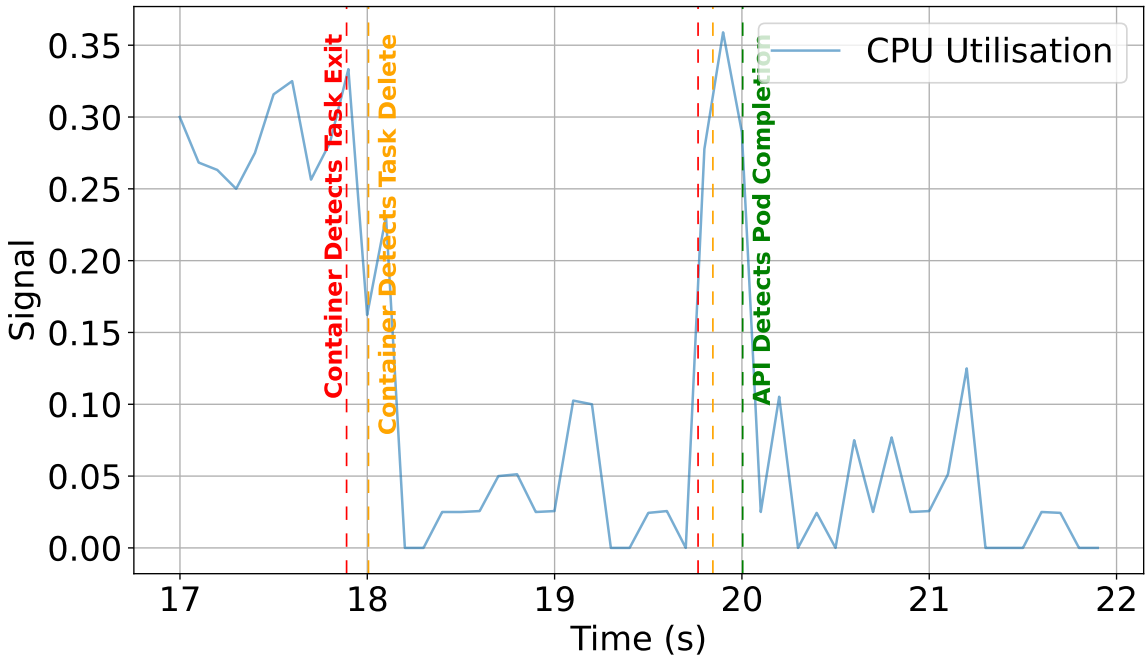

Figure 4.9: When different event listeners detected the completion of a Pod.

Figures 4.8 and 4.9 show that communication latency from the Kubernetes API causes its listener to miss container runtime resource spikes. Without forewarning, Nodes would incorporate these spikes into their predictions. On the other hand, we can see that certain container events precede the spikes. Though more complex, handling ContainerD events directly provides earlier warnings, reducing noise in calculations.

Estimating Pod-Cost

To produce a **reservable** signal, as per Section 3.5, Carico requires Nodes to estimate their baseline Capacity and Per-Pod-Cost. has the capability of estimating its capacity and per-Pod cost. I needed a streaming signal processing technique with a low-overhead and the ability to work with a dynamic system (handle changes in workloads over time). A Kalman filter [] is a powerful algorithm used for estimating the true state of a dynamic from a series of noisy and uncertain measurements. It's widely applied in fields like navigation (GPS), robotics, signal processing and control systems. Its ability to estimate a system's state from noisy measurements makes it suitable for this dynamic environment.

I devised three Kalman filter-based approaches to estimating reservation costs.

- 1D Kalman Filter predicting reservation cost based on the function:

$$\Delta\text{signal} = \Delta\text{no. of running Pods} \times \text{cost}$$

- 2D Kalman Filter to predict the signal based on the function:

$$\text{signal} = \text{capacity} + \text{per Pod cost} \times \text{no. of Pods}$$

- Two separate 1D Kalman Filters predicting the equation:

$$\text{signal} = \text{capacity} + \text{per Pod cost} \times \text{no. of Pods}$$

  Here, each filter learns a separate variable. This separation prevents non-zero covariance entries in the state covariance matrix ($\mathbf{P}$), mitigating oscillations observed with a single 2D Kalman filter.

To smooth out predictions, I employed two techniques. First, upon detecting container churn via the event listener, the Carico Pod temporarily halts estimations. Second, estimations are halted if the Capacity signal reaches zero. When the capacity signal is 0, it indicates that at least one resource is at capacity. If this occurs and another Pod begins running on the same Node, the signal still outputs 0. Otherwise, the filters might inaccurately decrease the Per-Pod-Cost, leading to an inflated advertised capacity.

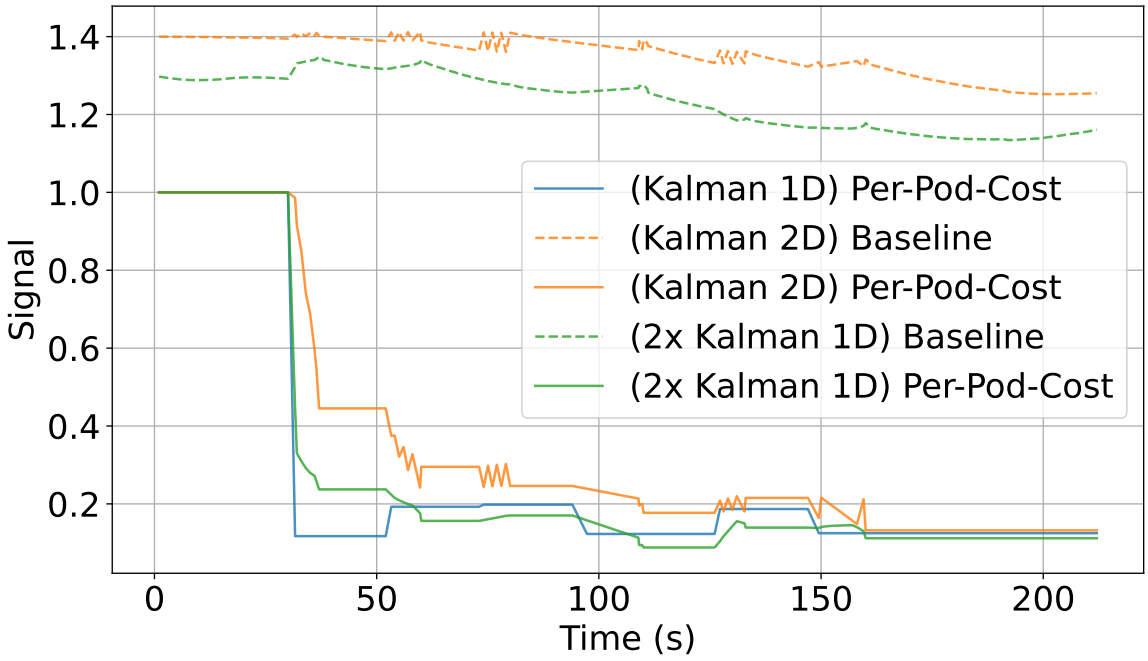

Figure 4.10: The estimates of the Kalman filters when Node experiences variable-sized bursts of `bpi(2000)` Pods.

To decide the optimal approach, I observed each methods' behaviour when executing Jobs of various sizes. This is depicted in Figure 4.10. The Δ-based Kalman filter accurately estimated Per-Pod-Cost, but being one-dimensional, could not estimate the Node's

baseline Capacity signal. The 2D Kalman filter approach provides a simple method for estimating both the Node's capacity and its per-Pod cost. Faster convergence for the 2D filter was attempted using large process noise covariance ($\mathbf{Q}$) values. This, however, led to large oscillations, as the filter adjusted both baseline capacity and cost variables to correct errors. The dual 1D Kalman filter was inspired by the stability of the 1D Kalman filter. This filter converged quickly and accurately without exhibiting the oscillations that plagued the 2D Kalman filter.

4.3 Aggregation Server

PRONTO aggregation resembles the distributed agglomerative summary model (DASM) []. Local models are aggregated in a "bottom-up" approach following a tree-structure depicted in Figure 2.2. While this approach reportedly requires minimal synchonisation, it demands multiple dedicated Pods, and Kubernetes' inherent communication latency could significantly delay global model updates after workload changes.

Therefore, I opted for a "flat" on-the-fly aggregation approach: when the Aggregation Server receives an aggregation request with a Node's local model, instead of aggregating the local model and returning the new global model, the server first enqueues the local model to be aggregated and returns its current view of the global model. This implementation trades consistency for latency.

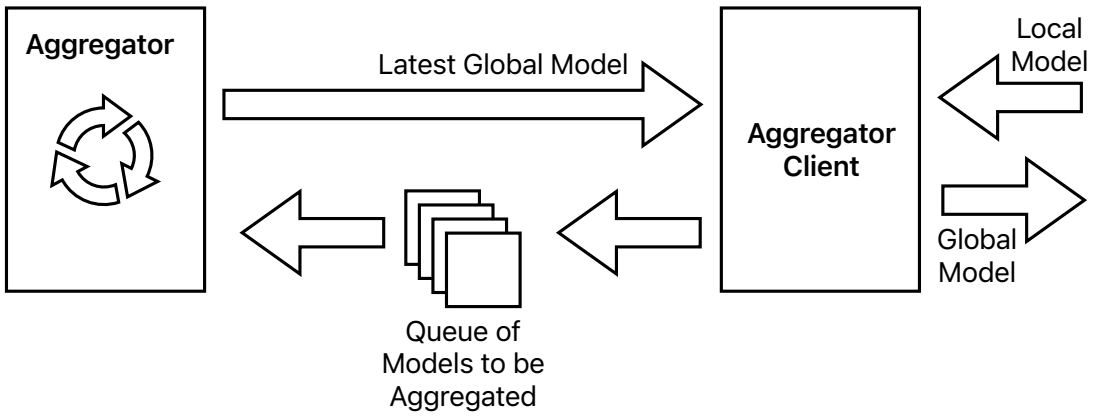

Figure 4.11: The components within the Aggregator Server.

The Aggregation Server executes a thread which waits on a queue of local models to aggregate. When the queue is non-empty, the thread pops the local model and performs a Subspace Merge operation (as defined in 3.3). To balance the influence of each local model, weights $\gamma_{\mathbf{A}} = \#$ of Nodes $- 1$ and $\gamma_{\mathbf{B}} = 1$ are used in the Subspace-Merge (as per Section 3.3). Aggregation clients perform a gRPC call to the address specified by

the Aggregation Service. This gRPC function is implemented by the server and takes the local model of a Node as its argument. The function first enqueues the local model to be merged and returns the latest view of the global model. Clients then aggregate their own local model with the received global model. Decoupling model aggregation from the gRPC call's critical path reduces server load, improving its capacity to handle more clients.

4.4 Scheduler Pod

4.4.1 Kubernetes Scheduler Plugin

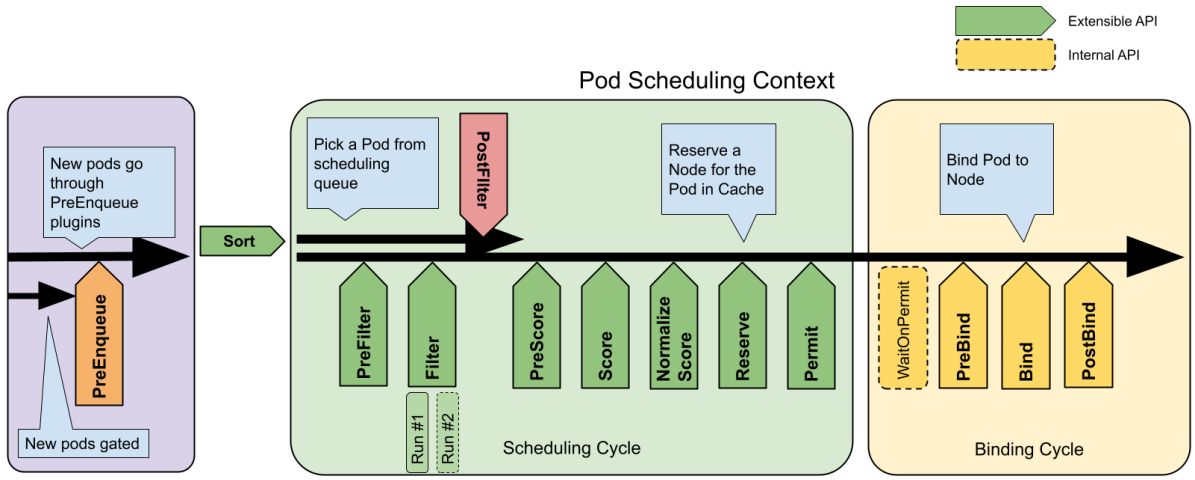

Figure 4.12: The available scheduling framework extension points [33].

The scheduling framework (depicted in Figure 4.12) is a pluggable architecture for the Kubernetes scheduler. It defines extension points at which scheduler plugins register to be invoked. A scheduler plugin can register to multiple extension points, with each extension point defining an interface: a set of functions the scheduler plugin has to implement.

Developing a CARICO-based scheduler plugin, rather than a standalone scheduelr, simplified implemention and offered many performance benefits. First, CARICO's scheduling operations (Section 3.5 map well to the framework's extension points. Second, the framework provides access to efficient, pre-existing data structures and algorithms. Finally, plugins allow customisation through selective enabling/disabling of default plugins and ordering of custom ones. This means that the CARICO plugin could be used in tandem with other plugins to improve scheduling decisions.

The CARICO scheduler tracks Pod reservations using a `map` (Pod ID to Node ID) and a Kubernetes API Pod Event Listener. During the Reserve phase, the scheduler increments the target Node's reserve count and records Pod-Node assignment. When the API listener

detects a Pod transitioning from the 'Pending' status, if the Pod is in its reservation `map`, the scheduler decrements the corresponding Node's reserved count.

Chapter 5

Evaluation

This section is focused on the empirical evaluation of Carico as a Kubernetes scheduler, comparing it against the default industry-standard `kube-schedulers`. I was unable to compare Carico against any similar telemetric-only schedulers due to their limited number and time constraints. For the evaluation, I use a set of common scheduling objectives used by datacenter providers [**?**]:

Job Completion - Section 5.3:
Schedulers often aim to reduce the time it takes for a job or a set of jobs to complete. In Kubernetes, Jobs are specified by a template of the Pods to be executed, the total number of Pods to complete (`completions`) and the maximum number of Pods running at once (`parallelism`). Job completion is defined as the time between a Job object being published to the Kubernetes API and the time when the last Pod of the Job completes. During the experiments, I set `parallelism` to `completions` so that only `kube-scheduler`'s decisions impact Job completion.

Pod Completion - Section 5.4:
The goal of many datacenter schedulers is to complete jobs as fast as possible so that resources are freed for subsequent jobs. For this section, I investigate the distribution of Pod Completion, the time it takes from when a Pod starts running to when it completes. In addition, I explain my findings using traces of the number of concurrent Pods on each Node during job execution.

Resource Utilisation - Section 5.5:
Since resources are expensive, datacenters aim to ensure that resources are well utilised with efficient placements. Over-utilisation can result in large amounts of resource thrashing, which wastes resources and hurts a datacenters proffitability. As Carico currently only uses CPU and memory metrics for scheduling, I only measured the utilisation of those resources during the exection of Jobs.

Workload Heterogeneity - Section 5.6:

As outlined in **??**, datacenters must handle workloads with different characteristics, such as, resource usage and running times. In this section, I evaluate how well Carico is able to handle mutliple Jobs with different characteristics.

Workload Isolation - Section 5.7:
Datacenters have to deal with jobs with different QoS requirements. One of these requirements is workload isolation: the execution of one Job will not interfere with the execution of another. With this property, users can be guaranteed a minimum level of quality.

Overhead - Section 5.8:
Due to the limited number of resources that need to be shared between users, datacenter providers aim to mitigate the overhead from scheduling. A lower overhead means more resources are available for users and providers can achieve higher profits margins. For this experiment, I measure the overhead incurred from running the DaemonSet of Carico Pods.

To ensure a fair comparison between Carico (telemetric-only scheduler) and `kube-scheduler` (resource description-based scheduler), I use a range of resource requests with `kube-scheduler` to highlight how much the performance can vary with different resource request.

5.1 Evaluation Setup

These experiments ran on a Kubernetes cluster containing 20 virtual machines (VMs) running on the Xen hypervisor. One of the machines is used as the master Node, and the rest are worker Nodes. The master Node contains all the Pods in the control plane, and during the evaluation of Carico, it contains the Carico Scheduler and Aggregation Server. Each VM features four Intel Xeon Gold 6142 CPUs 2.60Ghz with 8 GB of RAM running Ubuntu 24.04.2 LTS. Each CPU has a single core with hyperthreading disabled. When running `kubectl describe nodes`, each Node advertises 4000 milli-CPU seconds and 8GB of RAM.

During the evaluation, I use a Prometheus deployment [] to collect various statistics, such as running Pod count, resource utilisation and Kubernetes object completions.

5.2 Experimental Workloads

During the experiments I used very short-lived workloads; workloads that take less than a minute to complete. While datacenters can expect to receive longer-running workloads, using them in the evaluation was not feasilble due to limited time and the need to run experiments multiple times. Short-lived tasks can still provide valuable insights into the performance of a scheduler. Due to their short completion time, the cost of poor scheduling decisions becomes more significant and easier to observe.

During this evaluation, I used two types of workloads:

1. `pi-2000`: A short-lived CPU-focused workload where a Pod computes the value of π to 2000 decimal points.

2. `sklearn`: A longer-running workload with a larger memory footprint. This Pod executes a script which uses `sklearn` which trains a small neural network classifier (512 features, 16 classes, 8 hidden layers each containing 1024 neurons) on 5000 randomly generated samples before running inference on another set of 5000 randomly generated samples.

Investigating metrics when running `pi-2000` and `sklearn` Jobs separately demonstrates how Carico handles opposing resource usage characteristics (CPU-focused vs memory-focused). Furthermore, when executing both these Jobs concurrently, the difference in runtime helps investigate how Carico also handles workloads with differnt running times.

In this experiment, I use a Job that specifies Pods that performed a small ML workload. This workload uses a significant amount of memory, which unlike CPU, must be carefully handled. If we increase the number of processes on a fully-utilised CPU, it only results in each process having a smaller portion of CPU time and degrading its performance. On the other hand, memory is less forgiving as once memory runs out, the kernel begins OOM killing processes. This be detrimental to Job Completion, as terminated Pods results in wasted computations.

5.3 Job Completion

Figure 5.1 demonstrates the Job completion of `pi-2000` with different Pod counts. We can observe that Carico is able to consistently achieve comparable Job completions (within $\approx$ 10% of the optimal run with `kube-scheduler`). From Figure **??**, we can see how much the performance of the default scheduler varies depending on the amount of CPU time requested. Over-estimating requests can result in the CPU being underutilised, while under-estimating can result in too many Pods running on a Node at once. With Carico, we observed only observed a 10% reduction in Job Completion time. This can be attributed to its use of telemetric data: CPU utilisation amd CPU Pressure. In Section 4.2.1, I investigated these metrics and showed how with `bpi(2000)` Pods, these metrics indicated full capacity when running 4-8 Pods. As the capacity signal of a Node is tied to these metrics, the Node's will never advertise more capacity than $\approx$ 8 Pods.

The Job Completions from the experiment are given in Table 5.2. Carico achieves a worse performance in the smaller 100 Pod Job, but actually overtakes the default Kubernetes scheduler with the 200 Pod Job.

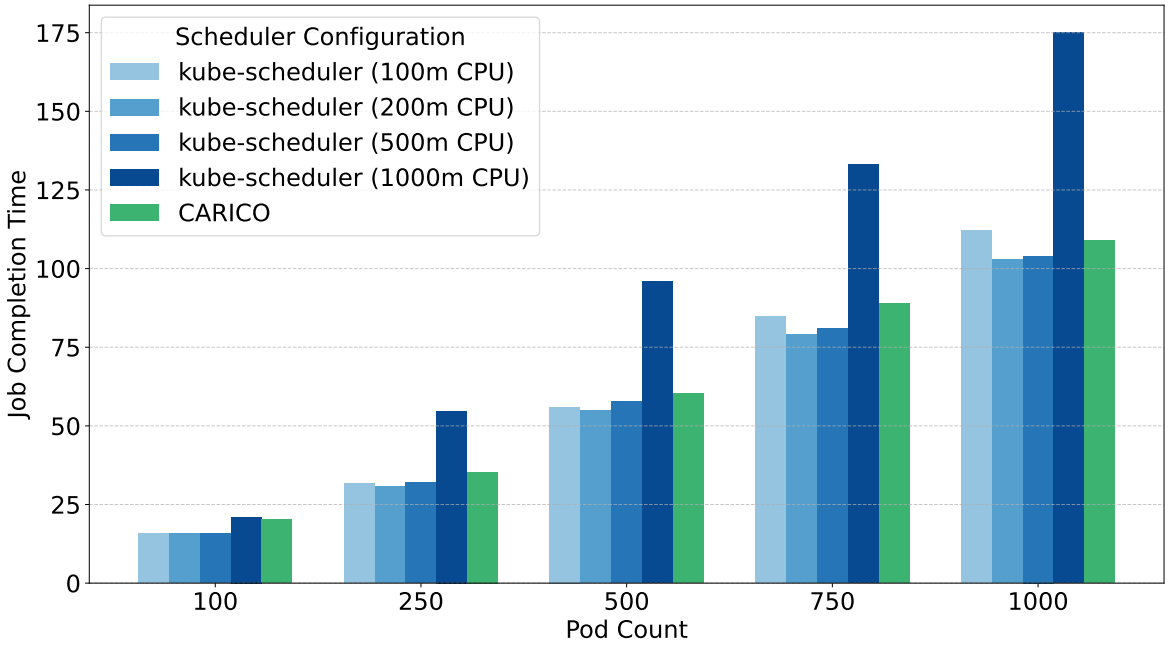

Figure 5.1: Job Completion of Job deployments with different Pod counts. Each Pod executed `bpi(2000)`. For the default scheduler, the requested resources are also given

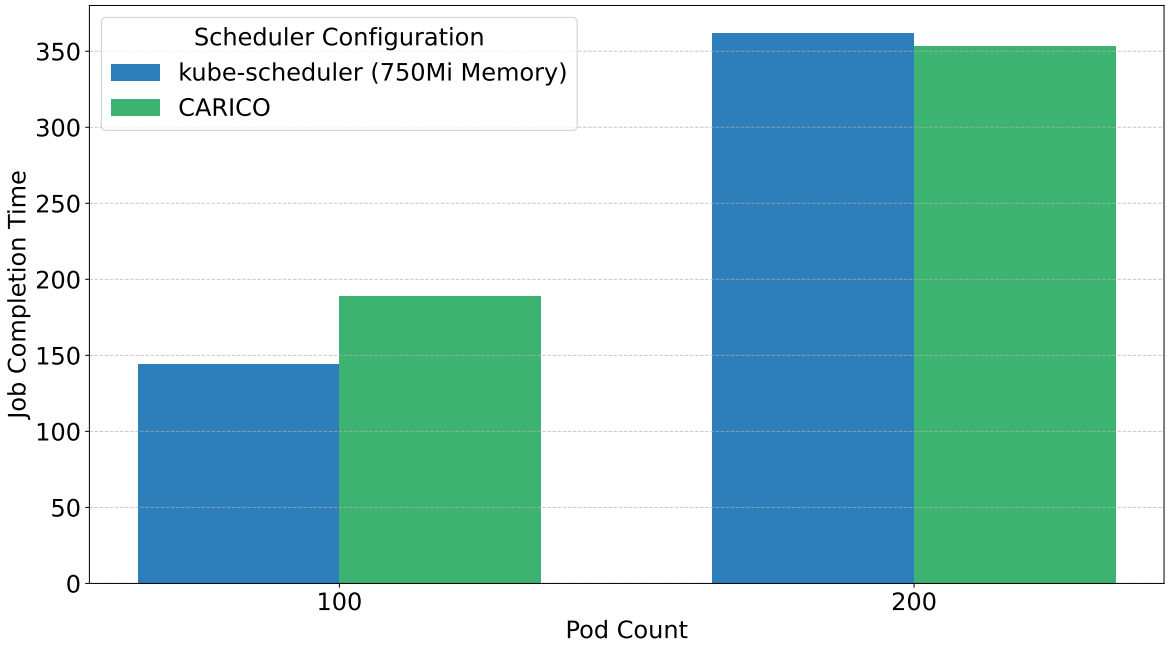

Figure 5.2: Job Completion of Job deployments with different Pod counts. Each Pod executed a small ML workload. For the default scheduler, the requested resources are also given

Scheduler	CPU Request	Mean	Std.	Min.	25%	Median	75%	Max.
Default	100m	47.43	14.59	7.00	39.00	52.00	57.00	73.00
Default	500m	9.55	1.49	5.00	9.00	10.00	10.00	14.00
Carico		7.69	0.99	5.00	7.00	8.00	8.00	11.00

Table 5.1: Pod Completion of multi-resource Job deployments with different Pod counts. For the default scheduler, `bpi(2000)` Pods requested 100 milliseconds of CPU and ML Pods requested 200 milliseconds CPU and 750Mi of memory

5.4 Pod Completion

I decided to further investigate the behaviour of the schedulers by measuring the Pod Completion time given in Figure 5.1. From this table, we observe that the lower request default schedulers ends up with a very tail-heavy distribution for Pod Completions. Increasing the request to 500 milliseconds, reduces the mean by $\approx 80\%$ while also reducing the skew. However, Carico is able to achieve the lowest Pod Completion distribution. To help explain the reason by this result, I also measured the number of Pods running on each Nodes during the Job execution, and present the values in Figure 5.3.

Figure 5.3 depicts the different approaches taken by each scheduler. As the default Kubernetes Scheduler tackles scheduling as if it were a bin-packing problem, it schedules as many pods that can fit on a Node; each Node has 4000m CPU capacity, 1000m per core. As a result, the 100m request results in a stampede of Pods while the 500m request and Carico assign a relatively constant number of Pods. However, the default scheduler with 500m Pods takes the edge in terms of throughput as it achieves a higher number of running Pods per Node.

Scheduler	# Pods	Mean	Std.	Min.	25%	Median	75%	Max.
Default	100	127.38	5.29	118	123.00	126.00	132.00	138.00
Carico	100	59.02	14.62	27.00	55.00	61.00	66.00	94.00
Default	200	225.19	36.19	45.00	231.00	236.00	239.00	244.00
Carico	200	64.46	14.33	23.00	57.75	67.00	73.25	89.00

Table 5.2: Pod Completion of multi-resource Job deployments with different Pod counts. For the default scheduler, `bpi(2000)` Pods requested 100 milliseconds of CPU and ML Pods requested 200 milliseconds CPU and 750Mi of memory

Table 5.2 gives the Pod Completion Distribution of the ML-based Jobs. When using the default Kubernetes scheduler, increasing the Pod count in a Job where the resource request is underestimated, increases drastically the average Pod Completion time as well as skewing the distribution to become more tail-heavy. However, the distribution of Pod Completion Time achieved by Carico remains consistent as you increase the Job size.

Figure 5.4 depicts the number of Pods running on each Node at a given time. We can see how in the larger ML Job, the default scheduler is able to allocate a majority of the Pods across the Nodes. Each Node advertises $\approx$ 8GB of memory while each Pod

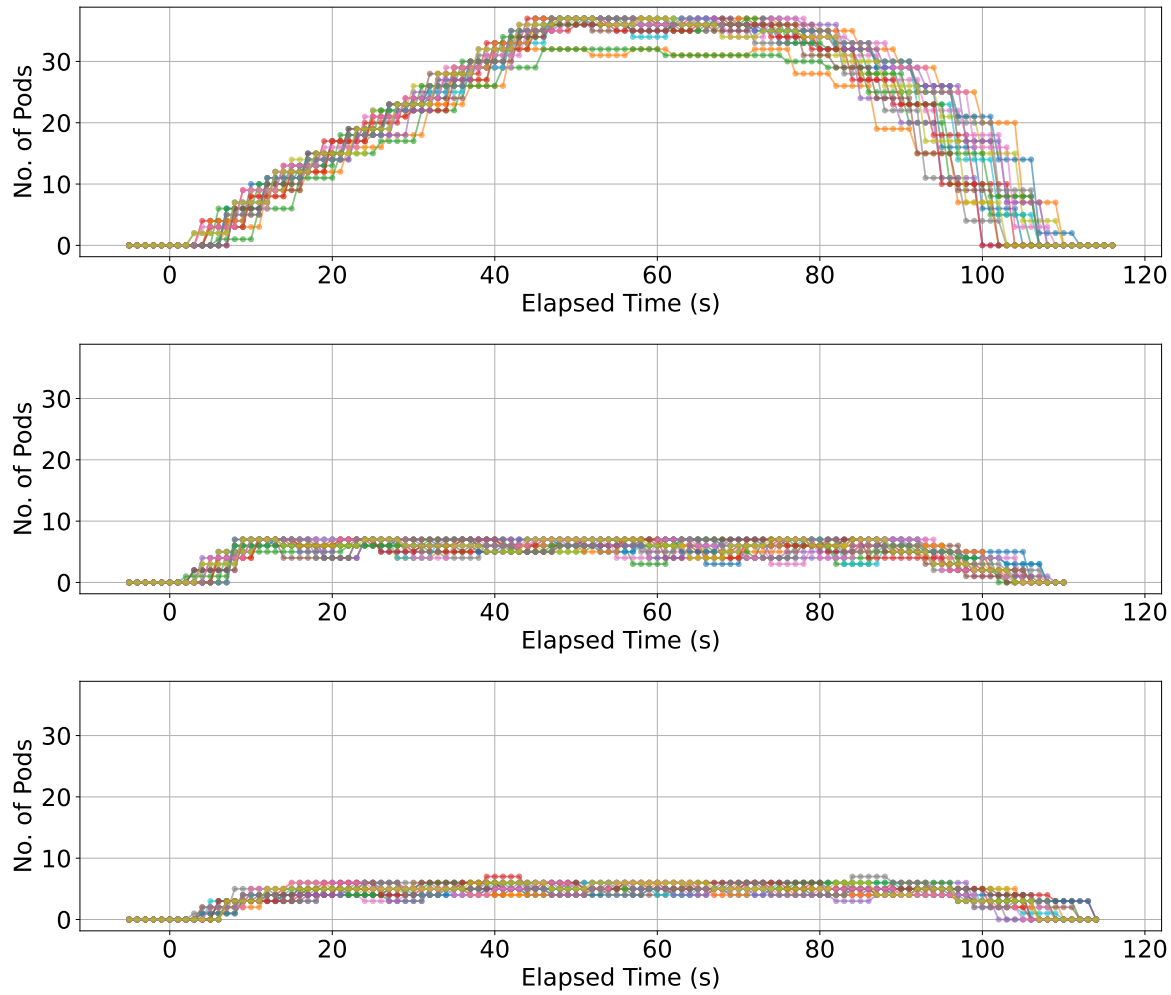

Figure 5.3: The number of `bpi(2000)` Pods running on a Node during the execution of a Job with 1000 Pods.

requests 750MiB of Memory. All these Pods end up competing for resources, and the overcontention increases individual Pod completion time. The scheduler still has to wait for Pods to terminate to free up memory. When space does become available, it is because a stampede of Pods have terminated. While, the scheduler was able to now allocate the remaining Pods, only a few Nodes are used while the rest become idle. This second wave of Pods results in a slower throughput compared Carico which ensures 1-3 Pods are always running on a Node.

5.5 Resource Utilisation

Figure 5.5 shows the resource utilisation during the execution of a Job with 1000 Pods. The default Kubernetes scheduler with 100m CPU requests achieves 100% CPU utilisation due to the large number of Pods running on each Node. The resulting allocation even results in a visible increase in the Memory usage.

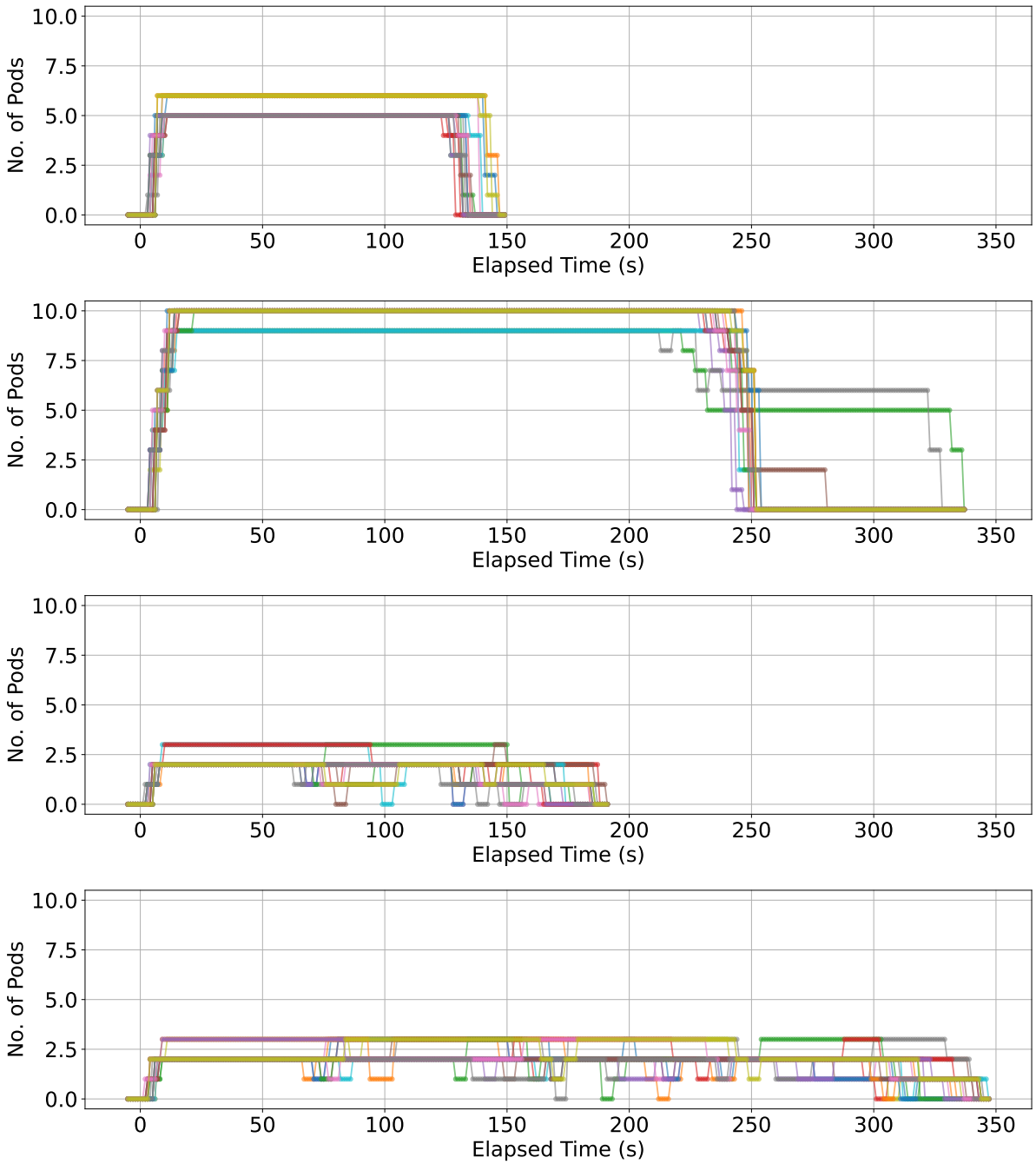

Figure 5.4: The number of ML Pods running on a Node during the execution of a Job with 100 and 200 Pods.

Figure 5.4 also helps to explain the resulting resource usage depicted in Figure 5.6. While the ML workload is memory-intense, it still contributes significantly to CPU utilisation. As the default scheduler does not actively look at resource utilisation, it is able to allocate Pods to Node's with fully-utilised CPUs. As a result, it achieves a higher memory usage with both Jobs. However, we can also observe the effect of the second wave of Pod allocations during the 200 Pod Job. During the last minute of the Job's executing, the average CPU and Memory utilisation of the cluster have dropped to $\approx 10\%$; barely above

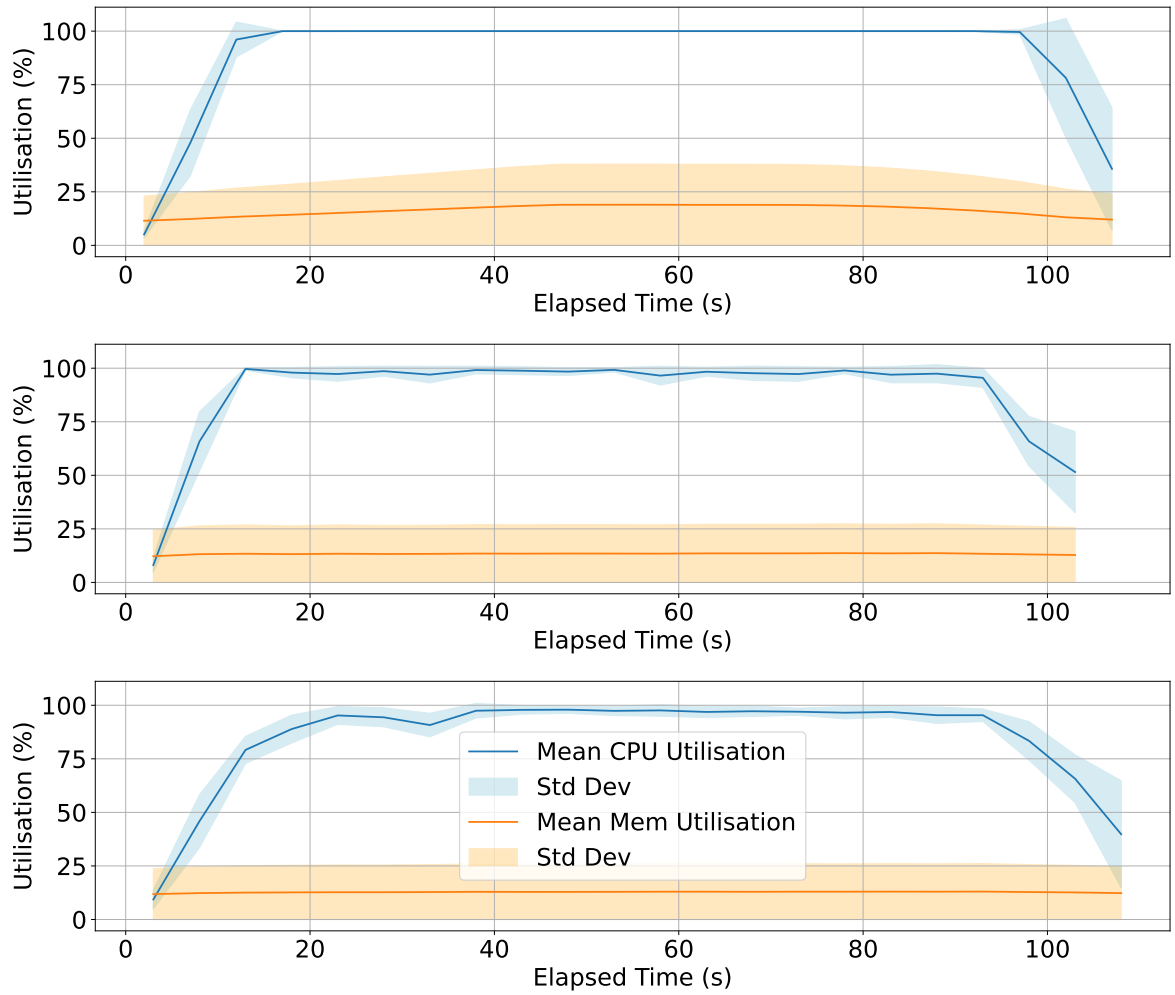

Figure 5.5: the resource utilisation when scheduling a job with 1000 pods executing `bpi(2000)`. the top figure gives the resource utilisation when scheduling with the default kubernetes scheduler. The bottom figure gives the resource utilisation when scheduling with spazio.

their baseline utilisation. On the other hand, Carico is again limited by the Node's CPU metrics, achieving a lower overall memory utilisation.

5.6 Workload Heterogeneity

In this experiment, I deployed the two Jobs defined above: a short-lived CPU-focused workload and a longer running ML workload. This experiment evaluates how Carico handles more than one type of workload.

5.6.1 Throughput

To thoroughly evaluate Carico in this scenario, I varied the distribution of Pods from each Job. The observed Job Completions are given in Table 5.7.

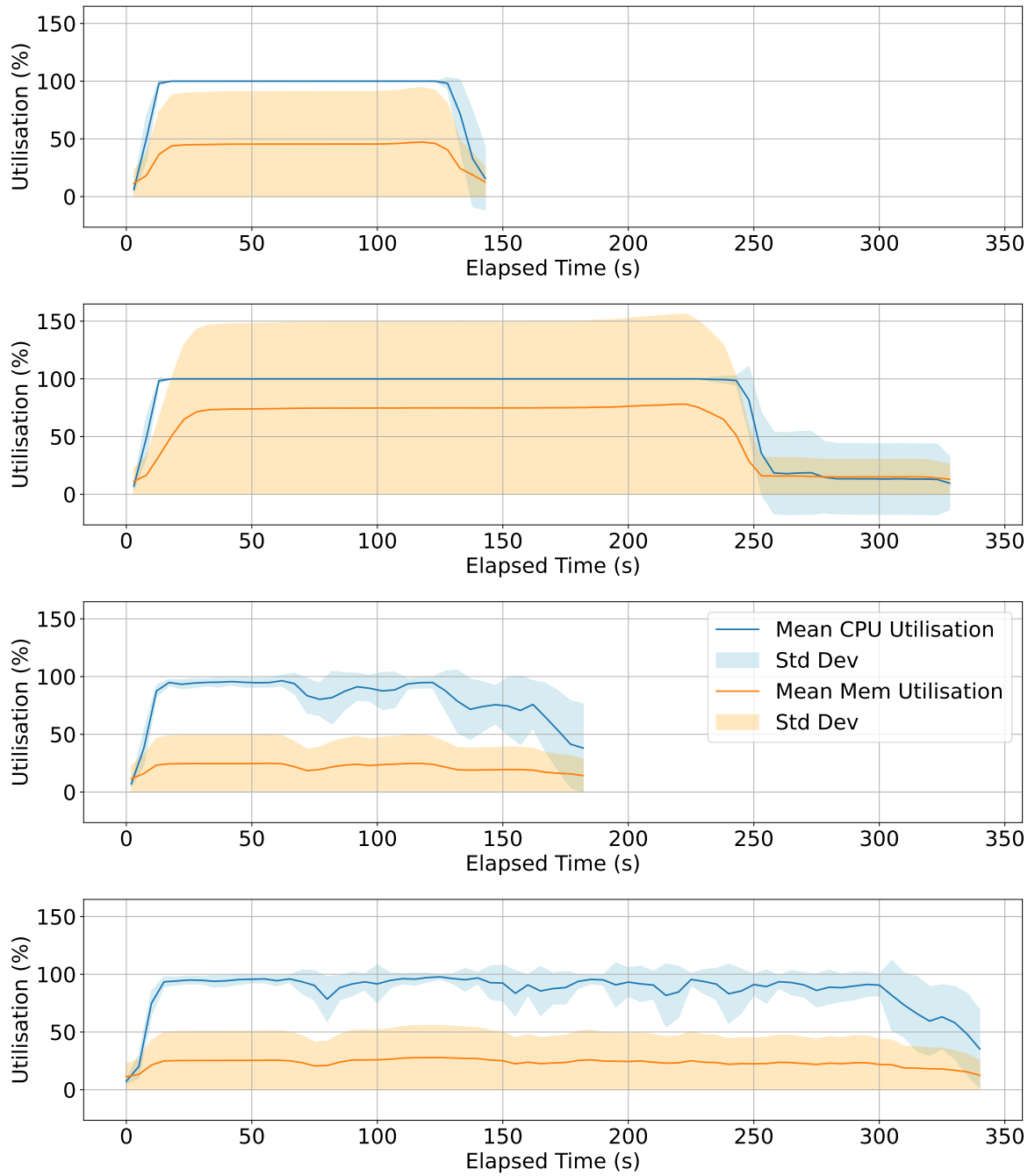

Figure 5.6: The resource utilisation when scheduling a Job with 1000 Pods executing `bpi(2000)`. The top figure gives the resource utilisation when scheduling with the default Kubernetes scheduler. The bottom figure gives the resource utilisation when scheduling with Carico.

The Job Completions from the experiment are given in Table 5.7. Carico achieves a higher throughput during the 500-20 and 250-50 combined workloads. However, the final 100-100, we see how the limiting throughput is now governed by the throughput achieved with the memory-centric workload.

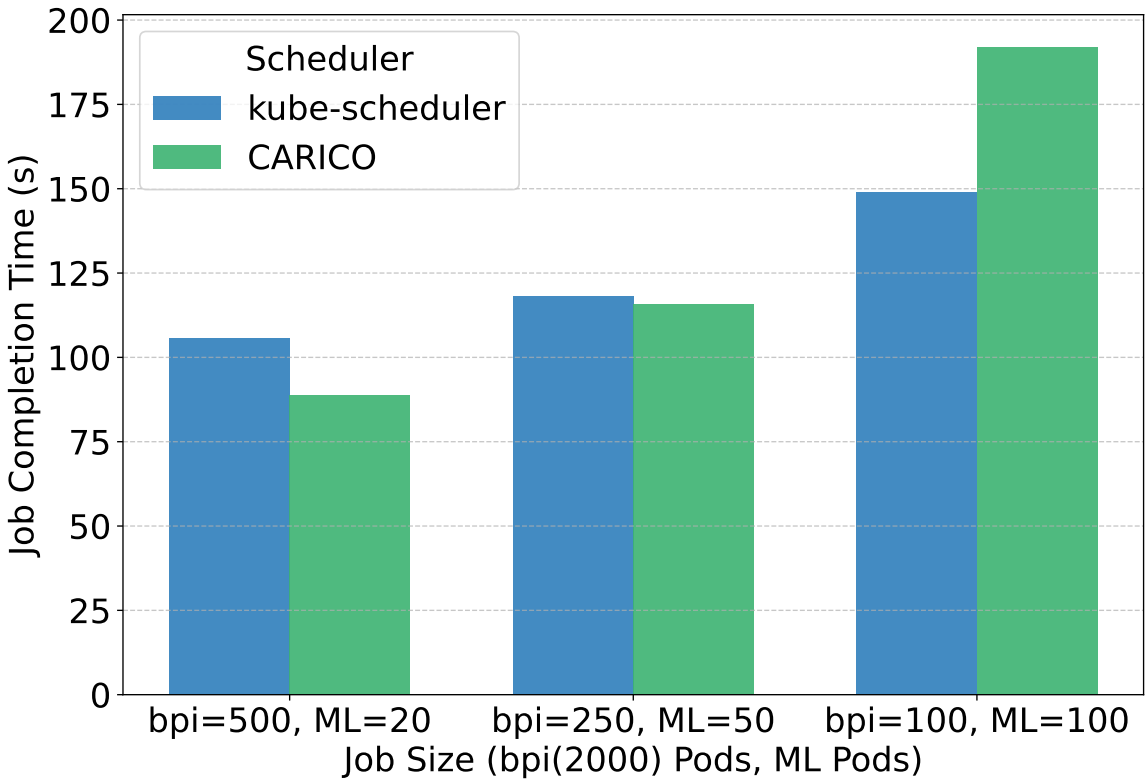

Figure 5.7: Job Completion of multi-resource Job deployments with different Pod counts. For the default scheduler, `bpi(2000)` Pods requested 100 milliseconds of CPU and ML Pods requested 200 milliseconds CPU and 750Mi of memory

5.6.2 Pod Completions

Due to Carico's lackluster throughput, I decided to investigate distribution of Pods across Nodes and how it impacted Pod Completion times.

Scheduler	Job	Mean	Std.	Min.	25%	Median	75%	Max.
Default	`pi-2000`	28.78	7.52	7.00	27.00	30.00	33.00	45.00
Default	ML	65.25	10.53	49.00	58.25	64.00	75.25	82.00
Carico	`pi-2000`	7.40	1.14	5.00	7.00	7.00	8.00	11.0
Carico	ML	34.50	7.39	22.00	27.50	36.00	40.25	44.00

Table 5.3: Pod Completion of multi-resource Job deployments with different Pod counts. For the default scheduler, `bpi(2000)` Pods requested 100 milliseconds of CPU and ML Pods requested 200 milliseconds CPU and 750Mi of memory

Table 5.3 gives the Pod Completion Distribution during an execution of the 500-20 Job combination. We can observe that the Pod Completion times for both Jobs is significantly higher with the default scheduler compared to Carico. This shows how Carico is still able to achieve a low-tailed Pod Completion time when scheduling workloads with different resource requests.

Figure 5.8 depicts the number of Pods running on each Node at a given time. Like in 5.4,

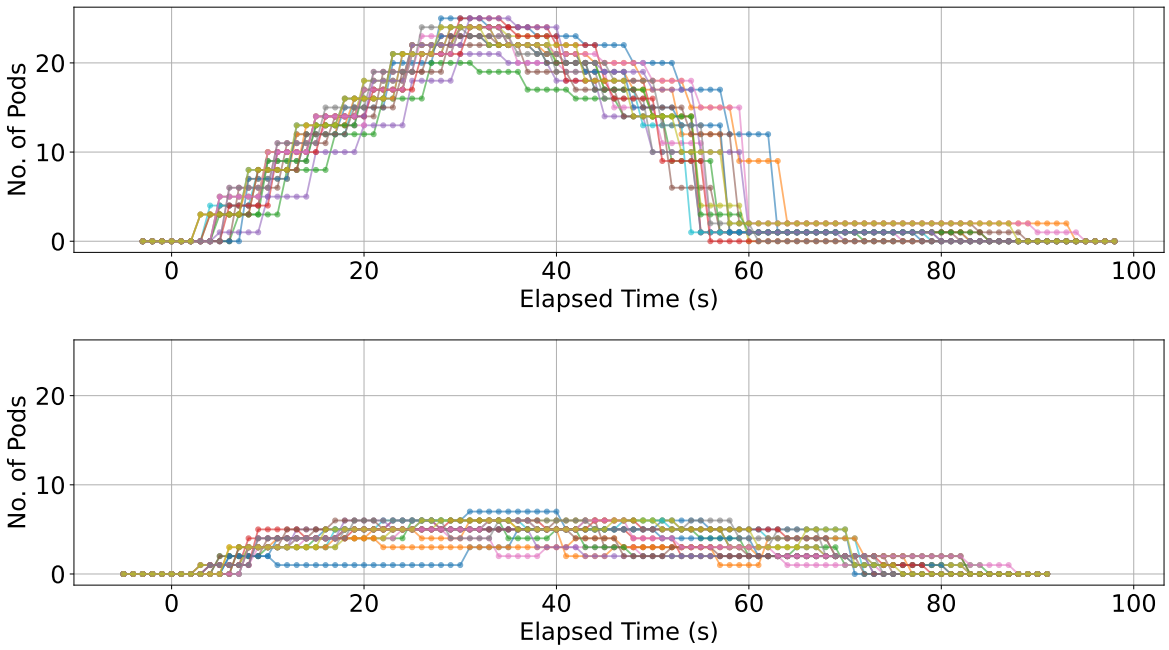

Figure 5.8: The number of Pods running on a Node during the 500-20 Job combination.

the default scheduler ends up with long-running Pods on small percentage of the Nodes in the cluster. The default scheduler see that the Node's have enough advertised capacity, and therefore, allocate all the Pods as they arrive. This again results in a stampede of completions, and only a few Nodes continue to do work. However, Carico's rate of Pod allocation remains consistent, ensuring that Nodes have a close to constant number of Pods.

5.6.3 Resource Utilisation

Figure 5.9 shows the resource utilisation running the 500-20 combined Jobs. For the same reasons as with the ML workload, the default scheduler ends up with a low resource utilisation for the latter portion of the Job exeuction. Instead, Carico achieves a more consistent resource utilisations, experiencing less of a fall in CPU utilisation near the end of the Job. In this scenario, Carico achieves a more efficient allocation of resources.

5.7 Workload Isolation

To evaluate Carico's QoS, I investigated how its scheduling decisions impact the performance of already running Pods. For this experiment, I had a Pod running on a worker Node, while another Pod periodically sent HTTP GET requests. This polling Pod would then measure latency of the response. I then scheduled a Job of 1000 Pods executing `bpi(2000)` across the cluster and measured how the response latency changed. In the default schedulers case, each Pod requested 100 milliseconds of CPU time.

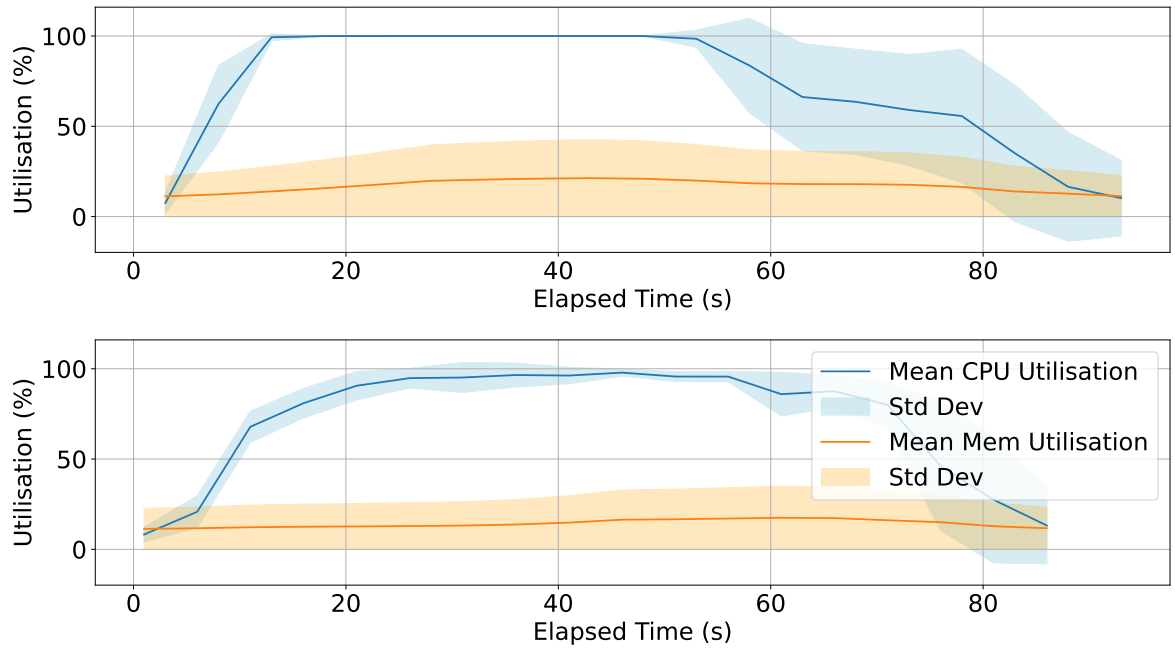

Figure 5.9: The resource utilisation when scheduling a Job with 1000 Pods executing `bpi(2000)`. The top figure gives the resource utilisation when scheduling with the default Kubernetes scheduler. The bottom figure gives the resource utilisation when scheduling with Carico.

Scenario	**Response Latency (ms)**					
	Min	**Med**	**P90**	**P95**	**P99**	**Max**
Baseline	0.99	3.04	3.78	4.00	4.47	8.32
Default Scheduler	1.07	10.06	18.61	22.28	28.82	54.49
Carico	1.00	2.48	6.09	7.82	10.53	17.39

Table 5.4: The distribution of a servers response latency when different schedulers attempt to allocate a 1000 Pod Job across the server.

Table 5.4 contains the measured distribution of the response latency from the server. It shows how scheduling with the default scheduler using 100m CPU requests, resulting a significant shift in latency distribution. The median more than doubles and the distribution greatly shifted towards the tail: the maximum latency was $\approx \times 7$ larger. On the other hand, when scheduling with Carico, the median latency actually decreased. Furthermore, while the tail distribution did increase, the max latency was only $\approx \times 2$ bigger.

5.8 Carico Overhead

To measure the overhead incurred from running the Carico pods on the Nodes, I compared the completion time of Jobs when running on Nodes with and without the Carico deployment. I considered easuring resource utilisation on a Node with just the Carico Pod running, but much of the behaviour of the Carico Pod occurs during container

events. As a result, the measured overhead would not represent the entire impact of the Carico Pod. Instead, by measuring the overhead over Jobs, we aggregate the impact of Carico across multiple container events, providing a more holistic view of its impact.

Number of Pods	% Overhead with Carico
100	-2.33 ± 3.29
250	-1.19 ± 2.44
500	4.84 ± 1.25
750	1.69 ± 0.42
1000	2.27 ± 0.66

Table 5.5: The overhead incurred when running Carico Pods on Nodes during the executing of Jobs with varying Pod counts. Each Pod executed `bpi(2000)` and requested 200 milliseconds of CPU time.

To measure Carico's overhead, I used Pod's executing `bpi(2000)`. Table 5.8 presents the relative change in Job Completion time with Carico Pods running on the Nodes. We can see that the Job Completion time of smaller Jobs are more noisy, therefore, resulting in an observed decrease in Job Completion times. However, with larger and more stable Jobs, the overhead from Carico is more visible. From these observations we can conclude that Carico has $\approx 2\%$ overhead.

5.9 Limitation

Limitations: *In this section, I will go over the limitations of the system. I will highlight how certain metrics like CPU-Utilisations don't give any more information once saturated. I will also have to mention how due to the sub-linear pod completion time, the Kubernetes scheduler is able to achieve higher job throughput by packing more pods into nodes.*

5.10 Summary

Summary: *In this section, I will summarise the results of my evaluation section, highlighting key findings and reasoning.*

Chapter 6

Conclusion and Future Work

6.1 Summary

The goal of this dissertation was to implement a telemetric-only Kubernetes scheduler using the theory behind PRONTO as a spring-board. I based the design of the scheduler behind PRONTO because of its federated nature and its use of contention-based metrics.

This dissertation resembles little to what was in the Project Proposal, and I feel this tells a lot about this project. A telemetric-only Kubernetes scheduler was a novel and inetresting presented an interesting and novel

6.2 Future Work

Bibliography

[1] Latest Kubernetes Adoption Statistics: Global Insights, May 2024. Section: Blog. URL: https://edgedelta.com/company/blog/kubernetes-adoption-statistics.

[2] Google Kubernetes Engine (GKE). URL: https://cloud.google.com/kubernetes-engine.

[3] schaffererin. What is Azure Kubernetes Service (AKS)? - Azure Kubernetes Service. URL: https://learn.microsoft.com/en-us/azure/aks/what-is-aks.

[4] Praneel Madabushini. Leveraging Kubernetes for AI/ML Workloads: Case studies in autonomous driving and large language model infrastructure. *World Journal of Advanced Engineering Technology and Sciences*, 15(1):1044–1052, January 2025. Publisher: GSC Online Press. URL: https://journalwjaets.com/node/480, doi:10.30574/wjaets.2025.15.1.0320.

[5] What is Kubernetes on Edge?, June 2024. URL: https://www.cloudraft.io/what-is/kubernetes-on-edge.

[6] Testimonials - Knative. URL: https://knative.dev/docs/about/testimonials/.

[7] Apache OpenWhisk is a serverless, open source cloud platform. URL: https://openwhisk.apache.org/.

[8] Kubernetes Cost Optimization: Strategies & Best Practices. URL: https://www.cloudbolt.io/cloud-cost-management/kubernetes-cost-optimization/.

[9] Nikhil Gopinath. Bin Packing and Cost Savings in Kubernetes Clusters on AWS. URL: https://www.sedai.io/blog/bin-packing-and-cost-savings-in-kubernetes-clusters-on-aws.

[10] Kubernetes Scheduler. Section: docs. URL: https://kubernetes.io/docs/concepts/scheduling-eviction/kube-scheduler/.

[11] Yixin Bao, Yanghua Peng, and Chuan Wu. Deep learning-based job placement in distributed machine learning clusters. In *IEEE INFOCOM 2019-IEEE conference on computer communications*, pages 505–513. IEEE, 2019.

[12] Yanghua Peng, Yixin Bao, Yangrui Chen, Chuan Wu, Chen Meng, and Wei Lin. Dl2: A deep learning-driven scheduler for deep learning clusters. *IEEE Transactions on Parallel and Distributed Systems*, 32(8):1947–1960, 2021.

[13] Ying Yang and Lijun Chen. Design of kubernetes scheduling strategy based on lstm and grey model. In *2019 IEEE 14th International Conference on Intelligent Systems and Knowledge Engineering (ISKE)*, pages 701–707. IEEE, 2019.

[14] Andreas Grammenos, Evangelia Kalyvianaki, and Peter Pietzuch. Pronto: Federated Task Scheduling, April 2021. arXiv:2104.13429 [cs]. URL: `http://arxiv.org/abs/2104.13429`, `doi:10.48550/arXiv.2104.13429`.

[15] Abdul Qadeer. Scaling Kubernetes to Over 4k Nodes and 200k Pods, January 2022. URL: `https://medium.com/paypal-tech/scaling-kubernetes-to-over-4k-nodes-and-200k-pods-29988fad6ed`.

[16] Kubernetes Components. Section: docs. URL: `https://kubernetes.io/docs/concepts/overview/components/`.

[17] Gilbert Strang. *Introduction to Linear Algebra*. Wellesley-Cambridge Press, 2009.

[18] Armin Eftekhari, Raphael A Hauser, and Andreas Grammenos. Moses: A streaming algorithm for linear dimensionality reduction. *IEEE transactions on pattern analysis and machine intelligence*, 42(11):2901–2911, 2019.

[19] Ionel Gog, Malte Schwarzkopf, Adam Gleave, Robert N. M. Watson, and Steven Hand. Firmament: fast, centralized cluster scheduling at scale. In *Proceedings of the 12th USENIX conference on Operating Systems Design and Implementation*, OSDI'16, pages 99–115, USA, November 2016. USENIX Association.

[20] Francescomaria Faticanti, Daniele Santoro, Silvio Cretti, and Domenico Siracusa. An application of kubernetes cluster federation in fog computing. In *2021 24th Conference on Innovation in Clouds, Internet and Networks and Workshops (ICIN)*, pages 89–91. IEEE, 2021.

[21] Daniele Santoro, Daniel Zozin, Daniele Pizzolli, Francesco De Pellegrini, and Silvio Cretti. Foggy: A platform for workload orchestration in a fog computing environment. In *2017 IEEE International Conference on Cloud Computing Technology and Science (CloudCom)*, pages 231–234. IEEE, 2017.

[22] Angel Beltre, Pankaj Saha, and Madhusudhan Govindaraju. Kubesphere: An approach to multi-tenant fair scheduling for kubernetes clusters. In *2019 IEEE cloud summit*, pages 14–20. IEEE, 2019.

[23] Muhammad Fadhriga Bestari, Achmad Imam Kistijantoro, and Anggrahita Bayu Sasmita. Dynamic resource scheduler for distributed deep learning training in ku-

bernetes. In *2020 7th International Conference on Advance Informatics: Concepts, Theory and Applications (ICAICTA)*, pages 1–6. IEEE, 2020.

[24] Marcos Carvalho and Daniel Fernandes Macedo. Qoe-aware container scheduler for co-located cloud environments. In *2021 IFIP/IEEE International Symposium on Integrated Network Management (IM)*, pages 286–294. IEEE, 2021.

[25] László Toka. Ultra-reliable and low-latency computing in the edge with kubernetes. *Journal of Grid Computing*, 19(3):31, 2021.

[26] Carmen Carrión. Kubernetes scheduling: Taxonomy, ongoing issues and challenges. *ACM Computing Surveys*, 55(7):1–37, 2022.

[27] Jiaming Huang, Chuming Xiao, and Weigang Wu. Rlsk: A job scheduler for federated kubernetes clusters based on reinforcement learning. In *2020 IEEE International Conference on Cloud Engineering (IC2E)*, pages 116–123. IEEE, 2020.

[28] Yiwen Han, Shihao Shen, Xiaofei Wang, Shiqiang Wang, and Victor CM Leung. Tailored learning-based scheduling for kubernetes-oriented edge-cloud system. In *IEEE INFOCOM 2021-IEEE conference on computer communications*, pages 1–10. IEEE, 2021.

[29] Ishak Harichane, Sid Ahmed Makhlouf, and Ghalem Belalem. A proposal of kubernetes scheduler using machine-learning on cpu/gpu cluster. In *Computer Science On-line Conference*, pages 567–580. Springer, 2020.

[30] Apache Hadoop. Apache hadoop yarn. *The Apache Software Foundation*, 2016.

[31] Shalmali Sahasrabudhe and Shilpa S. Sonawani. Improved filter-weight algorithm for utilization-aware resource scheduling in OpenStack. In *2015 International Conference on Information Processing (ICIP)*, pages 43–47, December 2015. URL: `https://ieeexplore.ieee.org/document/7489348/`, `doi:10.1109/INFOP.2015.7489348`.

[32] proc_stat(5) - Linux manual page. URL: `https://www.man7.org/linux/man-pages/man5/proc_stat.5.html`.

[33] Scheduling Framework. Section: docs. URL: `https://kubernetes.io/docs/concepts/scheduling-eviction/scheduling-framework/`.

Appendix A

Required Lemmas for Model Interpretation

A.1 Proof: The First Left Singular Vector as a Pseudo Weighted Average

Let $\mathbf{A}$ be an $m \times n$ matrix with non-negative elements $0 \leq a_{ij} \leq 1$. Let u_1 be the first left singular vector and σ_1 the corresponding singular value of $\mathbf{A}$.

A.1.1 Fundamental Representation of u_1

The vector u_1 is an eigenvector of $\mathbf{A}\mathbf{A}^T$ associated with the largest eigenvalue σ_1^2: $\mathbf{A}\mathbf{A}^T = \sigma_1^2 u_1$. Let a_j denote the j-th column of $\mathbf{A}$. Then $\mathbf{A}\mathbf{A}^T = \sum_{j=1}^n a_j a_j^T$. Substituting this into the eigenvalue equation and assuming $\sigma_1 \neq 0$: $\left(\sum_{j=1}^n a_j a_j^T\right) u_1 = \sigma_1^2 u_1 \implies \sum_{j=1}^n a_j (a_j^T u_1) = \sigma_1^2 u_1$. Thus u_1 can be expressed as a linear combination of the columns of $\mathbf{A}$:

$$u_1 = \sum_{j=1}^{n} \left(\frac{a_j^T u_1}{\sigma_1^2} \right) a_j = \sum_{j=1}^{n} w_j a_j, \text{ where } w_j = \frac{a_j^T u_1}{\sigma_1^2}$$

A.1.2 Contribution of Columns to u_1

The magnitude of each weight w_j is given by:

$$|w_j| = \frac{|a_j^T u_1|}{\sigma_1^2} = \frac{\| a_j \| \, |\cos(\theta_j)|}{\sigma_1^2}$$

where θ_j is the angle between column a_j and u_1. Columns a_j with larger norms $\| a_j \|$ or those more parallel to u_1 (i.e. $|\cos(\theta_j)| \approx 1$) will have weights w_j of greater magnitude. Consequently, these "larger" or more aligned columns contribute more significantly to the sum defining u_1 and thus to its direction

A.1.3 Non-Uniqueness of u_1 and Relation to Perron-Frobenius Theorem

The singular vectors in SVD are not unique: if $\mathbf{A} = \mathbf{U}_1\Sigma\mathbf{V}_1^T = \mathbf{U}_2\Sigma\mathbf{V}_2^T$ then $\Sigma_1 = \Sigma_2$ but $\mathbf{U}_1 = \mathbf{U}_2\mathbf{B}_a$ and $\mathbf{V}_1 = \mathbf{V}_2\mathbf{B}_b$ for some block diagonal unitary matrices $\mathbf{B}_a, \mathbf{B}_b$ [18].

Since $\mathbf{A}$ has non-negative entries ($a_{ij} \geq 0$), $\mathbf{A}\mathbf{A}^T$ is a non-negative matrix. By the Perron-Frobenius theorem, there exists an eigenvector u_1^+ corresponding to the eigenvalue σ_1^2 whose components u_{1i}^+ are all non-negative ($u_{1i}^+ \geq 0$). The first left singular vector u_1 obtained from SVD must then be $u_1 = bu_1^+$ where $b = \pm 1$

A.1.4 Interpretation as a Pseudo Weighted Average

- **Case 1:** $b = 1 \implies u_1 = u_1^+$.
  In this case, $a_j^T u_1 = a_j^T u_1^+ = \sum_i a_{ij} u_{1i}^+ \geq 0$ (as $a_{ij} \geq 0, u_{1i}^+ \geq 0$).
  The weights $w_j = (a_j^T u_1)/\sigma_1^2$ are therefore non-negative ($w_j \geq 0$).
  $u_1 = \sum w_j a_j$ becomes a conic combination of the non-negative column vectors a_j. This u_1 (itself non-negative) acts as a pseudo weighted average, representing a principal direction within the cone spanned by the a_j. Columns contributing larger non-negative w_j pull u_1 more strongly in their direction.

- **Case 2:** $b = -1 \implies u_1 = -u_1^+$.
  Here, $a_j^T u_1 = a_j^T(-u_1^+) = -a_j^T(u_1^+) \leq 0$.
  The weights $w_j = (a_j^T u_1)/\sigma_1^2$ are non-positive ($w_j \leq 0$).
  While $u_1 = \sum w_j a_j$ now involves non-positive weights for non-negative vectors a_j, the magnitudes $|w_j| = (a_j^T u_1)/\sigma_1^2$ remain the same as in Case 1. Thus, columns a_j that are "larger" or more aligned with u_1^+ still contribute with greater magnitude to the sum, determining the orientation of the line spanned by u.

A.1.5 Conclusion

The vector u_1 is a linear combination of the columns of $\mathbf{A}$, $u_1 = \sum w_j a_j$. The magnitude of the coefficient w_j for each column a_j is proportional to the projection of a_j onto u_1 (scaled by $1/\sigma_1^2$). This means the columns with larger norms or those more aligned with the principal direction (the line spanned by u_1) contribute more significantly to defining this direction.

Irrespective of the sign b (determined by the SVD algorithm), the line along which u_1 lies is shaped by this weighted aggregation.

A.2 Proof: Monotonicity of the First Singular Value for Non-Negative Matrices

Let $\mathbf{A}$ and $\mathbf{B}$ be $m \times n$ matrices with real entries such that $0 \leq a_{ij} \leq b_{ij} \leq 1$ for all i, j. We want to show that $\sigma_1(\mathbf{A}) \leq \sigma_1(\mathbf{B})$, where $\sigma_1(\mathbf{M})$ denotes the first (largest) singular value of a matrix $\mathbf{M}$.

A.2.1 Relating Singular Values to $\mathbf{M}^T\mathbf{M}$

The square of the first singular value, $\sigma_1(\mathbf{M})^2$, is the largest eigenvalue of the matrix $\mathbf{M}^T\mathbf{M}$. Since $\mathbf{M}^T\mathbf{M}$ is a symmetric positive semi-definite matrix, its largest eigenvalue is also its spectral radius, $\rho(\mathbf{M}^T\mathbf{M})$. Thus, $\rho(\mathbf{A})^2 = \rho(\mathbf{A}^T\mathbf{A})$ and $\rho(\mathbf{B})^2 = \rho(\mathbf{B}^T\mathbf{B})$.

A.2.2 Comparing $\mathbf{A}^T\mathbf{A}$ and $\mathbf{B}^T\mathbf{B}$

Let $\mathbf{M_A} = \mathbf{A}^T\mathbf{A}$ and $\mathbf{M_B} = \mathbf{B}^T\mathbf{B}$. The (j, k)-th element of thess matrices are:

$$(\mathbf{M_A})_{jk} = \sum_{i=1}^{m} a_{ij}a_{ik} \tag{A.1}$$

$$(\mathbf{M_B})_{jk} = \sum_{i=1}^{m} b_{ij}b_{ik} \tag{A.2}$$

Since $0 \leq a_{ij} \leq b_{ij}$ for all i, j:

- All a_{ij} and b_{ij} are non-negative
- Therefore, $a_{ij}a_{ik} \leq b_{ij}b_{ik}$ for all i, j, k. Summing over i:

$$\sum_{i=1}^{m} a_{ij}a_{ik} \leq \sum_{i=1}^{m} b_{ij}b_{ik}$$

  This implies $(\mathbf{M_A})_{jk} \leq (\mathbf{M_B})_{jk}$ for all j, k. Thus, $0 \leq \mathbf{M_A} \leq \mathbf{M_B}$ element-wise. Both $\mathbf{M_A}$ and $\mathbf{M_B}$ are matrices with non-negative entries.

A.2.3 Monotonicity of Spectral Radius

A standard result from Perron-Frobenius theory states that if $\mathbf{X}$ and $\mathbf{Y}$ are non-negative matrices such that $\mathbf{X} \leq \mathbf{Y}$ element-wise, then their spectral radii satisfy $\rho(\mathbf{X}) \leq \rho(\mathbf{Y})$. Applying this result to $\mathbf{M_A} = \mathbf{A}^T\mathbf{A}$ and $\mathbf{M_B} = \mathbf{B}^T\mathbf{B}$:

$$\rho(\mathbf{A}^T\mathbf{A}) \leq \rho(\mathbf{B}^T\mathbf{B})$$

A.2.4 Conclusion

From Section A.2.1 and A.2.3:

$$\sigma_1(\mathbf{A})^2 \leq \sigma_1(\mathbf{B})^2$$

Since the singular values are by definition non-negative ($\sigma_1(\mathbf{M}) \geq 0$):

$$\sigma_1(\mathbf{A}) \leq \sigma_1(\mathbf{B})$$

This shows that if the values of a non-negative matrix $\mathbf{A}$ are increased (while remaining non-negative, e.g., elements between 0 and 1), the first singular value of the resulting matrix $\mathbf{B}$ wil greater than or equal to that of $\mathbf{A}$.

A.3 Proof: Singular Value of Concatenated Matrix

This section proves the following statement:
Given two non-negative matrices $\mathbf{A} \in \mathbb{R}^{m \times n_1}$ and $\mathbf{B} \in \mathbb{R}^{m \times n_2}$, the first singular value of the concatenated matrix $\mathbf{C} = [\mathbf{A}, \mathbf{B}]$ is greater than or equal to the maximum of the first singular values of $\mathbf{A}$ and $\mathbf{B}$. That is,

$$\sigma_1([\mathbf{A}, \mathbf{B}]) \geq \max(\sigma_1(\mathbf{A}), \sigma_1(\mathbf{B}))$$

A.3.1 Setup

Let $\mathbf{A}$ be an $m \times n_1$ matrix and $\mathbf{B}$ be an $m \times n_2$ matrix. The concatenated matrix $\mathbf{C} = [\mathbf{A}, \mathbf{B}]$ is an $m \times (n_1 + n_2)$ matrix. The first singular value of any matrix $\mathbf{M}$, denoted $\sigma_1(\mathbf{M})$, is defined as its spectral norm:

$$\sigma_1(\mathbf{M}) = \| \mathbf{M} \|_2 = \max_{\|x\|_2 = 1} \| \mathbf{M}x \|_2$$

where x is a unit vector.

A.3.2 Relating $\sigma_1(\mathbf{C})$ to $\sigma_1(\mathbf{A})$

Let $v_{\mathbf{A}}^*$ be a unit vector in $\mathbb{R}^{n_1}$ such that $\sigma_1(\mathbf{A}) = \| \mathbf{A}v_{\mathbf{A}}^* \|_2$. Such a vector $v_{\mathbf{A}}^*$ is the right singular vector corresponding to $\sigma_1(\mathbf{A})$.

Consider a vector $x_0 \in \mathbb{R}^{n_1+n_2}$ constructs as $x_0 = \begin{bmatrix} v_{\mathbf{A}}^* \\ 0_{n_2 \times 1} \end{bmatrix}$, where $0_{n_2 \times 1}$ is the zero vector of dimensions n_2.
The squared norm of x_0 is $\| x_0 \|_2^2 = \| v_{\mathbf{A}}^* \|_2^2 + \| 0_{n_2 \times 1} \|_2^2 = 1^2 + 0 = 1$. Thus, x_0 is a unit vector.

By definitions of $\sigma_1(\mathbf{C})$:

$$\sigma_1(\mathbf{C}) = \max_{\|x\|_2=1} \| \mathbf{C}x \|_2$$

Since x_0 is a specific unit vector, we have:

$$\sigma_1(\mathbf{C}) \geq \| \mathbf{C}x_0 \|_2$$

Computing $\mathbf{C}x_0$ gives:

$$\mathbf{C}x_0 = [\mathbf{A}, \mathbf{B}] \begin{bmatrix} v_{\mathbf{A}}^* \\ 0_{n_2 \times 1} \end{bmatrix} = \mathbf{A}v_{\mathbf{A}}^* + \mathbf{B}\dot{0}_{n_2 \times 1} = \mathbf{A}v_{\mathbf{A}}^*$$

Therefore,

$$\sigma_1(\mathbf{C}) \geq \| \mathbf{A}v_{\mathbf{A}}^* \|_2 = \sigma_1(\mathbf{A})$$

A.3.3 Relating $\sigma_1(\mathbf{C})$ to $\sigma_1(\mathbf{B})$

Similarly, let $v_{\mathbf{B}}^*$ be a unit vector in $\mathbb{R}^{n_2}$ such that $\sigma_1(\mathbf{B}) = \| \mathbf{B}v_{\mathbf{B}}^* \|_2$. Such

Consider a vector $x_1 \in \mathbb{R}^{n_1+n_2}$ constructs as $x_1 = \begin{bmatrix} 0_{n_1 \times 1} \\ v_{\mathbf{B}}^* \end{bmatrix}$.
The squared norm of x_1 is $\| x_1 \|_2^2 = \| 0_{n_1 \times 1} \|_2^2 + \| v_{\mathbf{B}}^* \|_2^2 = 0 + 1^2 = 1$. Thus, x_1 is a unit vector.

Again, by definitions of $\sigma_1(\mathbf{C})$:

$$\sigma_1(\mathbf{C}) \geq \| \mathbf{C}x_1 \|_2$$

Computing $\mathbf{C}x_1$ gives:

$$\mathbf{C}x_1 = [\mathbf{A}, \mathbf{B}] \begin{bmatrix} 0_{n_1 \times 1} \\ v_{\mathbf{B}}^* \end{bmatrix} = \mathbf{A}\dot{0}_{n_1 \times 1} + \mathbf{B}v_{\mathbf{B}}^* = \mathbf{B}v_{\mathbf{B}}^*$$

Therefore,

$$\sigma_1(\mathbf{C}) \geq \| \mathbf{B}v_{\mathbf{B}}^* \|_2 = \sigma_1(\mathbf{B})$$

A.3.4 Conclusion

From Sections A.3.2 and A.3.3, we have shown that $\sigma_1(\mathbf{C}) \geq \sigma_1(\mathbf{A})$ and $\sigma_1(\mathbf{C}) \geq \sigma_1(\mathbf{B})$. This implies that $\sigma_1(\mathbf{C})$ must be greater than or equal to the maximum of these two values:

$$\sigma_1([\mathbf{A}, \mathbf{B}]) \geq \max(\sigma_1(\mathbf{A}), \sigma_1(\mathbf{B}))$$

A.4 σ_1 of Scaled Concatenation

This section proves the following statement: Given two non-negative matrices $\mathbf{A} \in \mathbb{R}^{m \times n_1}$ and $\mathbf{B} \in \mathbb{R}^{m \times n_2}$ and non-negative scalar weights $\gamma_{\mathbf{A}} = \sqrt{w_{\mathbf{A}}}$ and $\gamma_{\mathbf{B}} = \sqrt{w_{\mathbf{B}}}$ such that $w_{\mathbf{A}} + w_{\mathbf{B}} = 1$, the resulting first singular value and the first left singular vector of the concatenated matrix $\mathbf{C} = [\gamma_{\mathbf{A}}\mathbf{A}, \gamma_{\mathbf{B}}\mathbf{B}]$ has the following property:

$$\min(P_{\mathbf{A}}(u_{\mathbf{C}}), P_{\mathbf{B}}(u_{\mathbf{C}})) \leq \sigma_{\mathbf{C}}^2 \leq \max(P_{\mathbf{A}}(u_{\mathbf{C}}), P_{\mathbf{B}}(u_{\mathbf{C}}))$$

where $\sigma_{\mathbf{C}}$ and $u_{\mathbf{C}}$ correspond to the first singular value and first left singular vector of $\mathbf{C}$, $P_{\mathbf{M}}(u)$ is the sum of squared scalar porjections of the columns in $\mathbf{M}$ onto u (let m_j be the j-th column of $\mathbf{M}$ $P_{\mathbf{M}}(u) = \sum_{j=1}^{n}(u^T m_j)^2$).

A.4.1 Expanding $\sigma_1(\mathbf{C})$

By definition, $S_{\mathbf{C}} = \sigma_1(\mathbf{C})$ and $u_{\mathbf{C}}$ is the corresponding first singular left vector. Thus, they satisfy the eigenvalue equation for $\mathbf{C}\mathbf{C}^T$:

$$\mathbf{C}\mathbf{C}^T u_{\mathbf{C}} = S_{\mathbf{C}}^2 u_{\mathbf{C}}$$

Pre-multiplying by $u_{\mathbf{C}}^T$:

$$u_{\mathbf{C}}^T(\mathbf{C}\mathbf{C}^T u_{\mathbf{C}}) = u_{\mathbf{C}}^T(S_{\mathbf{C}}^2 u_{\mathbf{C}}) \tag{A.3}$$

$$u_{\mathbf{C}}^T\mathbf{C}\mathbf{C}^T u_{\mathbf{C}} = S_{\mathbf{C}}^2(u_{\mathbf{C}}^T u_{\mathbf{C}}) \tag{A.4}$$

Since $u_{\mathbf{C}}$ is a unit vector, $u_{\mathbf{C}}^T u_{\mathbf{C}} = \| u_{\mathbf{C}} \|_2^2 = 1$. So,

$$S_{\mathbf{C}}^2 = u_{\mathbf{C}}^T\mathbf{C}\mathbf{C}^T u_{\mathbf{C}}$$

Now, lets express $\mathbf{C}\mathbf{C}^T$ in terms of $\mathbf{A}$ and $\mathbf{B}$:
The matrix $\mathbf{C} = [\gamma_{\mathbf{A}}\mathbf{A}, \gamma_{\mathbf{B}}\mathbf{B}]$.
Then $\mathbf{C}^T = \begin{bmatrix} \gamma_{\mathbf{A}}\mathbf{A}^T \\ \gamma_{\mathbf{B}}\mathbf{B}^T \end{bmatrix}$.
So, $\mathbf{C}\mathbf{C}^T = [\gamma_{\mathbf{A}}\mathbf{A}, \gamma_{\mathbf{B}}\mathbf{B}] \begin{bmatrix} \gamma_{\mathbf{A}}\mathbf{A}^T \\ \gamma_{\mathbf{B}}\mathbf{B}^T \end{bmatrix} = (\gamma_{\mathbf{A}}\mathbf{A})(\gamma_{\mathbf{A}}\mathbf{A}^T) + (\gamma_{\mathbf{B}}\mathbf{B})(\gamma_{\mathbf{B}}\mathbf{B}^T)$

$$\mathbf{C}\mathbf{C}^T = \gamma_{\mathbf{A}}^2\mathbf{A}\mathbf{A}^T + \gamma_{\mathbf{B}}^2\mathbf{B}\mathbf{B}^T$$

Substitute this expression for $\mathbf{C}\mathbf{C}^T$ into the equation for $S_{\mathbf{C}}^2$:

$$S_{\mathbf{C}}^2 = u_{\mathbf{C}}^T(\gamma_{\mathbf{A}}^2\mathbf{A}\mathbf{A}^T + \gamma_{\mathbf{B}}^2\mathbf{B}\mathbf{B}^T)u_{\mathbf{C}} \tag{A.5}$$

$$S_{\mathbf{C}}^2 = \gamma_{\mathbf{A}}^2(u_{\mathbf{C}}^T\mathbf{A}\mathbf{A}^T u_{\mathbf{C}}) + \gamma_{\mathbf{B}}^2(u_{\mathbf{C}}^T\mathbf{A}\mathbf{A}^T u_{\mathbf{C}}) \tag{A.6}$$

Using the definitions for $P_{\mathbf{A}}(u_{\mathbf{C}})$ and $P_{\mathbf{B}}(u_{\mathbf{C}})$:

- $P_{\mathbf{A}}(u_{\mathbf{C}}) = u_{\mathbf{C}}^T \mathbf{A}\mathbf{A}^T u_{\mathbf{C}}$ (sum of squared projections of columns of $\mathbf{A}$ onto $u_{\mathbf{C}}$
- $P_{\mathbf{B}}(u_{\mathbf{C}}) = u_{\mathbf{C}}^T \mathbf{B}\mathbf{B}^T u_{\mathbf{C}}$ (sum of squared projections of columns of $\mathbf{B}$ onto $u_{\mathbf{C}}$

This means the equation becomes:

$$S_{\mathbf{C}}^2 = \gamma_{\mathbf{A}}^2 P_{\mathbf{A}}(u_{\mathbf{C}}) + \gamma_{\mathbf{B}}^2 P_{\mathbf{B}}(u_{\mathbf{C}})$$

We are given weights $\gamma_{\mathbf{A}}, \gamma_{\mathbf{B}}$ such that $\gamma_{\mathbf{A}}^2 \geq 0, \gamma_{\mathbf{B}}^2 \geq 0$, and $\gamma_{\mathbf{A}}^2 + \gamma_{\mathbf{B}}^2 = 1$. This means that $S_{\mathbf{C}}^2$ is a convex combination of the two values $P_{\mathbf{A}}(u_{\mathbf{C}})$ and $P_{\mathbf{B}}(u_{\mathbf{C}})$. A fundamental property of convex combinations is that they always lie between the minimum and maximum of the values being combined.
Let $x = P_{\mathbf{A}}(u_{\mathbf{C}})$ and $y = P_{\mathbf{B}}(u_{\mathbf{C}})$. Then $S_{\mathbf{C}}^2 = \gamma_{\mathbf{A}}^2 x + \gamma_{\mathbf{B}}^2 y$.
If $x \leq y$:

- $\min(x, y) = x = (\gamma_{\mathbf{A}}^2 + \gamma_{\mathbf{B}}^2)x = \gamma_{\mathbf{A}}^2 x + \gamma_{\mathbf{B}}^2 x \leq \gamma_{\mathbf{A}}^2 x + \gamma_{\mathbf{B}}^2 y = S_{\mathbf{C}}^2$ (since $\gamma_{\mathbf{B}}^2 \geq 0$ and $x \leq y$).
- $\max(x, y) = y = (\gamma_{\mathbf{A}}^2 + \gamma_{\mathbf{B}}^2)y = \gamma_{\mathbf{A}}^2 y + \gamma_{\mathbf{B}}^2 y \geq \gamma_{\mathbf{A}}^2 x + \gamma_{\mathbf{B}}^2 y = S_{\mathbf{C}}^2$ (since $\gamma_{\mathbf{A}}^2 \geq 0$ and $x \leq y$).

A similar argument holds if $y \leq x$. Therefore:

$$\min(P_{\mathbf{A}}(u_{\mathbf{C}}), P_{\mathbf{B}}(u_{\mathbf{C}})) \leq \sigma_{\mathbf{C}}^2 \leq \max(P_{\mathbf{A}}(u_{\mathbf{C}}), P_{\mathbf{B}}(u_{\mathbf{C}}))$$

Lorem ipsum dolor sit amet, consetetur sadipscing elitr, sed diam nonumy eirmod tempor invidunt ut labore et dolore magna aliquyam erat, sed diam voluptua. At vero eos et accusam et justo duo dolores et ea rebum. Stet clita kasd gubergren, no sea takimata sanctus est Lorem ipsum dolor sit amet. Lorem ipsum dolor sit amet, consetetur sadipscing elitr, sed diam nonumy eirmod tempor invidunt ut labore et dolore magna aliquyam erat, sed diam voluptua. At vero eos et accusam et justo duo dolores et ea rebum. Stet clita kasd gubergren, no sea takimata sanctus est Lorem ipsum dolor sit amet. Lorem ipsum dolor sit amet, consetetur sadipscing elitr, sed diam nonumy eirmod tempor invidunt ut labore et dolore magna aliquyam erat, sed diam voluptua. At vero eos et accusam et justo duo dolores et ea rebum. Stet clita kasd gubergren, no sea takimata sanctus est Lorem ipsum dolor sit amet.